JOURNAL OF MATERIALS SCIENCE 22 (1987) 1173–1192

# Crack propagation in ceramics under cyclic loads

L. EWART, S. SURESH
*Division of Engineering, Brown University, Providence, Rhode Island 02912, USA*

Stable crack growth is observed in notched plates of polycrystalline alumina subject to fully compressive far-field cyclic loads at room temperature in a moist air environment and *in vacuo*. The fatigue cracks propagate at a progressively decreasing velocity along the plane of the notch and in a direction macroscopically normal to the compression axis. The principal failure events leading to this effect are analysed in terms of notch-tip damage under the far-field compressive stress, microcracking, frictional sliding and opening of microcracks, and crack closure. An important contribution to such Mode I crack growth arises from the residual *tensile* stresses induced locally at the notch-tip when the deformation within the notch-tip process zone leaves permanent strains upon unloading from the maximum nominal compressive stress. It is shown that the phenomenon of crack growth under cyclic compressive stresses exhibits a macroscopically similar behaviour in a wide range of materials spanning the very ductile metals to extremely brittle solids, although the micromechanics of this effect are very different among the various classes of materials. The mechanisms of fatigue in ceramics are compared and contrasted with the more familiar examples of crack propagation under far-field cyclic compression in metallic systems and the implications for fracture in ceramic–metal composites and transformation toughened ceramic composites are highlighted. Strategies for some important applications of this phenomenon are recommended for the study of fracture mechanisms and for the measurement of fracture toughness in brittle solids.

## 1. Introduction

Ceramic materials have been the focus of increasing research activity in recent years as a result of their potential for extensive use in many engineering applications. One of the principal factors limiting the widespread application of ceramics in engineering structural components is their poor fracture properties. Considerable research work is currently in progress to explore various processes for improving the quasi-static fracture behaviour of brittle ceramics through intrinsic and extrinsic toughening mechanisms (e.g. [1]). An outstanding problem of scientific interest and practical significance is the ability of structural ceramics to withstand varying load patterns. Indeed, a clear understanding of the resistance to mechanical fatigue conditions is essential because high-frequency vibrations and load fluctuations can markedly affect the service life of structural ceramics. Despite its potential importance, the fracture behaviour of ceramics under cyclic loads had remained a relatively unexplored area of research.

A limited amount of prior work on the resistance of ceramics to fracture under tension–tension or tension–compression cyclic loads has led to a somewhat ambiguous picture of possible fatigue effects. In some studies, cyclic loads were found to result in a lower time to failure than static loads of a magnitude equal to the maximum fatigue load [2, 3]. While such observations imply the existence of a mechanical fatigue effect, other studies have shown that an intrinsic cyclic loading effect is either non-existent or occurs only in a very restricted range of temperature and loading conditions [4–10]. In some ceramic materials, such as polycrystalline $Si_3N_4$, soda–lime glass, and electrical porcelain containing $\sim 20\,\mu m$ quartz particulates, slow crack growth observed under varying load conditions has been interpreted to be a direct manifestation of stress corrosion cracking [7–10].

In a recent paper, Eward and Suresh [11] reported the discovery of mechanical fatigue fracture at room temperature in notched specimens of a single-phase polycrystalline aluminium oxide subject to fully compressive cyclic loads. This work revealed that even in the absence of appreciable macroscopic plasticity, stable Mode I fatigue crack propagation can occur in brittle solids at low temperatures [11]. In a parallel study, Suresh and Sylva [12] documented the occurrence of this phenomenon in cemented carbides. The objective of this paper is to discuss prominent characteristics of room-temperature fatigue crack growth in single crystals and polycrystals of aluminium oxide subject to fully compressive far-field cyclic loads. Possible effects of microcracking, residual stresses, grain size and crack wake contact on the fatigue fracture behaviour are examined. The mechanisms of failure in these brittle solids under cyclic compression loading conditions are compared and contrasted with the more familiar examples of fatigue crack propagation under far-field cyclic compression in metallic systems. We discuss experimental results describing

0022–2461/87 $03.00 + .12 

some important applications of the phenomenon of controlled crack initiation and growth under cyclic compression for the measurement of fracture toughness in brittle ceramics. Potential implications of this technique for the study of creep crack growth and high-temperature fatigue crack propagation thresholds in ceramics and their composites are also highlighted.

## 2. Materials and experimental methods

The ceramic materials investigated in this work consisted of two grades of polycrystalline aluminium oxide commercially available as AD 995 and AD 999 from Coors Porcelain Company, Boulder, Colorado. The former material has the following properties at room temperature: tensile strength = 260 MPa, compressive strength = 2620 MPa, Young's modulus = 372 GPa, specific gravity = 3.89, range of grain sizes = 2 to 50 $\mu$m and average grain size = 18 $\mu$m. The properties of AD 999 $Al_2O_3$ at room temperature are: tensile strength = 310 MPa, compressive strength = 3792 MPa, Young's modulus = 386 GPa, specific gravity = 3.96, range of grain sizes = 1 to 6 $\mu$m and average grain size = 3 $\mu$m. The AD 995 and AD 999 varieties are 99.5% and 99.9% pure aluminium oxide, respectively. The grain-boundary phase and impurities in these materials consist of $SiO_2$, MgO, calcium, sodium and iron. In order to evaluate the effects of crystallography on crack growth under cyclic loads and to compare with the results of polycrystalline $Al_2O_3$, compression fatigue experiments were also carried out in oriented sapphire ($\alpha$-$Al_2O_3$) crystals (obtained from Crystal Systems, Massachusetts).

Fatigue crack growth experiments under compression-to-compression loading conditions were carried out in single edge-notched specimens machined to the following dimensions: height = 37 mm, width = 15.9 mm, thickness = 9.4 mm, notch length = 6.3 mm and notch root radius = 0.75 mm. The notch was introduced using a diamond wheel. The single-crystal experiments were conducted with specimens containing notches parallel to the $\{0\,0\,0\,1\}$ and $\{1\,\bar{2}\,1\,0\}$ planes. Constant amplitude sinusoidal loads were applied to the specimens at a constant frequency of 20 Hz in a room temperature ($\sim 23^\circ$ C) moist air ($\sim 40\%$ relative humidity) environment. The load ratio $R$, defined as the ratio of minimum stress $\sigma^{\infty}_{min}$ to maximum stress $\sigma^{\infty}_{max}$ of the fatigue cycle, was 10 in all of the experiments. The load amplitude required to induce stable crack growth depends on the material microstructure and is reported along with the results for the various materials. Crack growth was monitored during the test on both the side surfaces of the specimen with the aid of an optical microscope. Final crack length through the thickness was observed both optically and in the scanning electron microscope after fracturing the specimens. In order to check whether fracture under cyclic loads is promoted by intrinsic mechanical fatigue damage (and not from possible stress corrosion effects induced by the moist air environment), compression-to-compression cyclic load experiments on polycrystalline $Al_2O_3$ were also carried out *in vacuo* ($\leqslant 10^{-4}$ Pa pressure).

## 3. Results on crack growth under cyclic compression

### 3.1. Polycrystalline $Al_2O_3$

The influence of cyclic compressive loads (stress amplitude $|\Delta\sigma^{\infty}| \approx 268$ MPa, $R = 10$) in the coarse grain microstructure of AD 995 is shown in Fig. 1. Here the discrete data sets A and B denote optically measured crack length on the two side surfaces of the specimen. The crack front was uniformly straight through the thickness of the specimen except very near (within about 0.5 mm) the two side surfaces where a greater extent of damage was observed. No crack propagation was detected beyond about $2.5 \times 10^5$ cycles. The total crack growth distance in the centre thickness sections was about 0.5 mm, whereas within about 0.5 mm of the two side surfaces the growth distance was about 0.75 mm (Fig. 1). A series of optical micrographs showing the changes in crack length on the two side surfaces, as a function of the number of compression cycles, is provided in Fig. 2.

A prominent feature of crack advance under imposed cyclic compression is the formation of particle debris within the crack. In order to assess the influence of crack wake contact (due to the accumulation of particles of $Al_2O_3$ removed by repeated contact in compression) on the rate of crack growth, a cyclic compression experiment was conducted with the AD 995 material where the specimen was ultrasonically cleaned after every 5000 compression cycles (all the loading conditions were identical to those used to obtain the results of Figs 1 and 2). Fig. 3 shows the progressive increase in fatigue crack length as a function of the compression cycles from such an experiment.

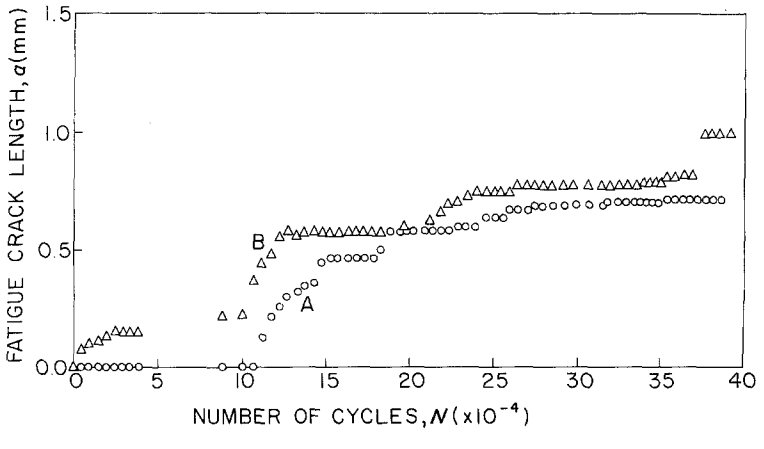


*Figure 1* Variation of fatigue crack length, $a$, measured from the notch-tip, as a function of the number of compression cycles, $N$, in AD 995 $Al_2O_3$. A and B refer to the crack length values optically measured on the two side surfaces of the specimen.

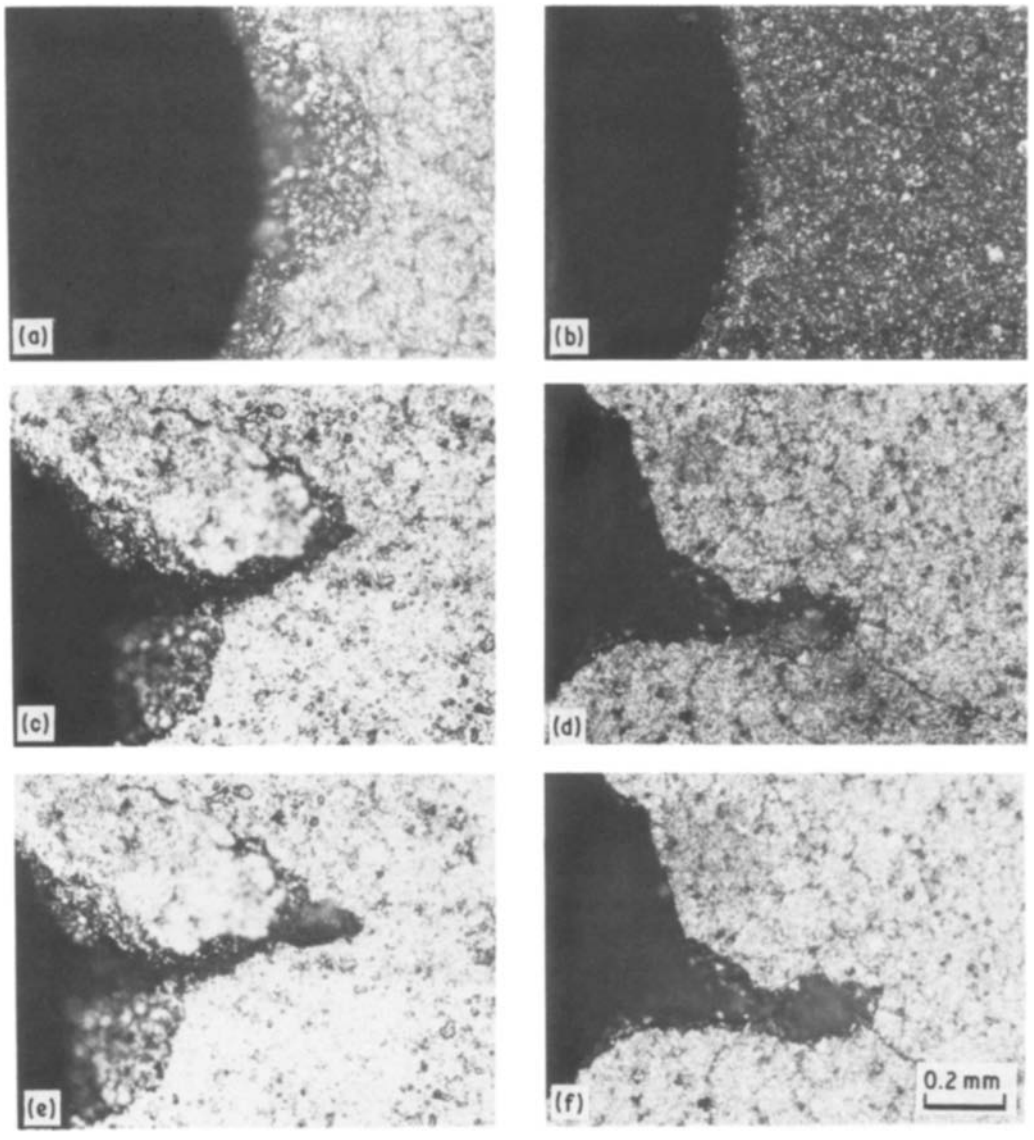


*Figure 2* A series of optical-micrographs showing the progressive increase in the length of a (macroscopically) Mode I crack on the two side surfaces (A and B) in AD 995 $Al_2O_3$. (a, b) $N$ = 0-; (c, d) $N$ = 201 000; (e, f) $N$ = 266 000. (a, c, e) Side A; (b, d, f) Side B.

A plot of the crack length against the number of compression cycles is provided in Fig. 4. The initial rate of crack growth through the thickness of the specimen is substantially greater than that observed in Fig. 1.

Fig. 5 is an optical micrograph showing the morphology of the crack propagated under compression-to-compression fatigue loads in the finer grain microstructure of AD 999. (Unless stated otherwise, all the results reported in this work pertain to experiments conducted without the periodic removal of particles from the crack.) The overall crack growth characteristics in this material were similar to those observed in AD 995 under far-field cyclic compression. However, an increase in compressive stress amplitude of about 50% was required to induce stable fatigue fracture in AD 999 over that for AD 995 under identical specimen geometry and testing conditions. Note that a direct comparison of the microstructural effects on crack growth *rates* between the two materials is not appropriate because of the differences in purity levels.

The occurrence of stable crack growth uniformly through the thickness of the specimen is illustrated by the optical micrograph in Fig. 6a. Higher-magnification micrographs of the crack-tip region in polycrystalline $Al_2O_3$ reveal a predominantly intergranular fracture path, as in Fig. 6b, for example. Fractographic observations on the failed surfaces also exhibit a similar trend. An interesting feature of crack advance in ceramics under far-field cyclic compression is the accumulation of debris particles formed within the crack during cyclic fracture (Fig. 6c). Such particles, of a maximum size of about 500 $\mu$m, are generated by fracture along the grain boundaries. The difference between the fatigue fracture surface and catastrophic quasi-static (bend) fracture surface is illustrated in Fig. 6d. The high-frequency contact between the mating crack faces is seen to result in a "flattening" of the fracture surface asperities during fatigue. Although the primary mechanism of cyclic fracture was intergranular separation, occasionally a small fraction of the grains observed on the fracture surface exhibited transgranular cleavage. Fig. 7a is a scanning electron fractograph of the compression fatigue fracture surface in AD 995. An examination of the central region at a higher magnification (Fig. 7b) reveals cleavage facets which appear to spread from the internal voids to the grain boundaries.

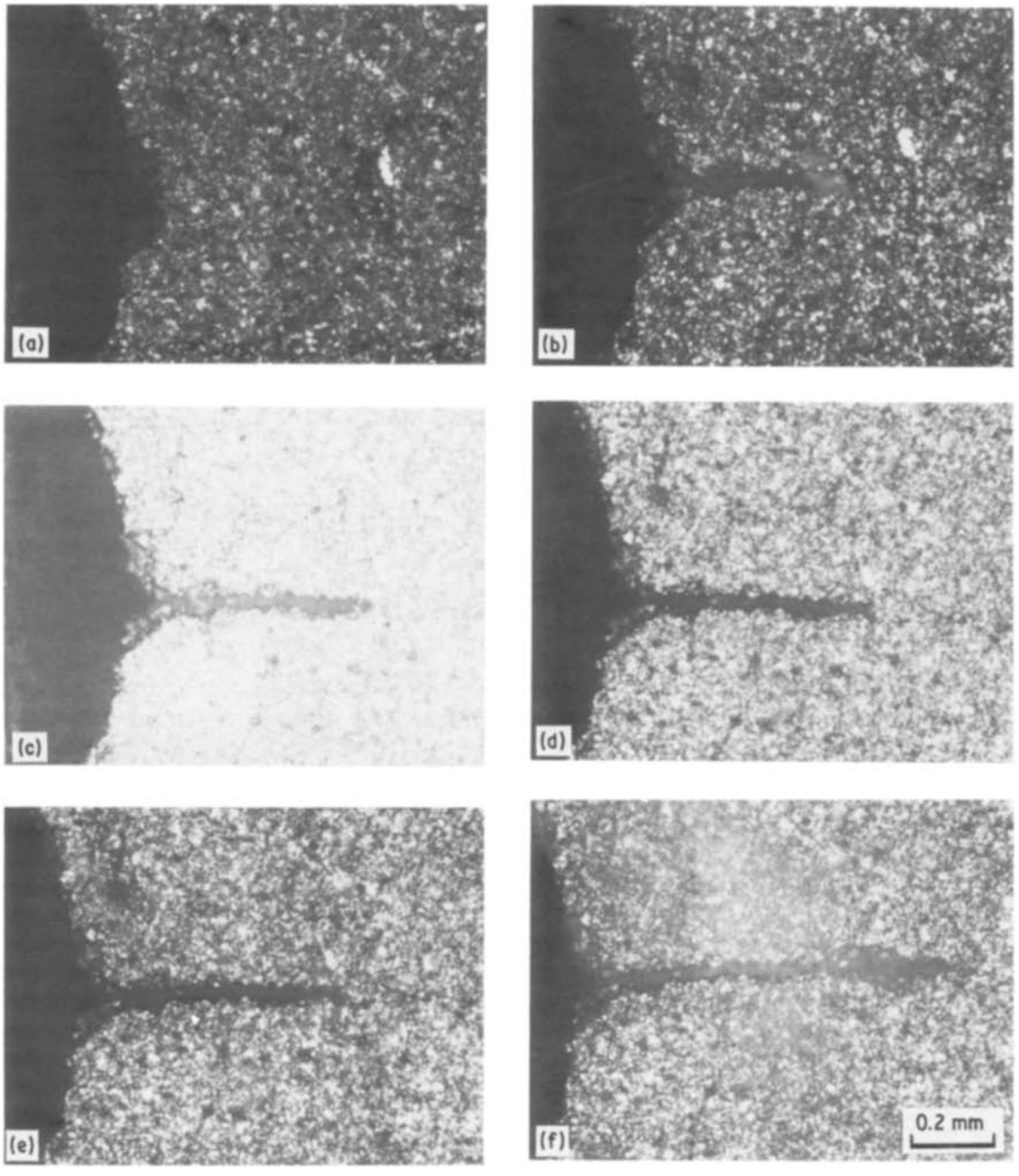


*Figure 3* A series of optical micrographs showing the progressive increase in crack length during compressive cycling in AD 995 $Al_2O_3$. The specimen was ultrasonically cleaned after every 5000 cycles in order to remove the particles from within the crack. Values of $N$: (a) 0; (b) 59 200, (c) 69 200, (d) 79 200, (e) 94 200, (f) 154 200.

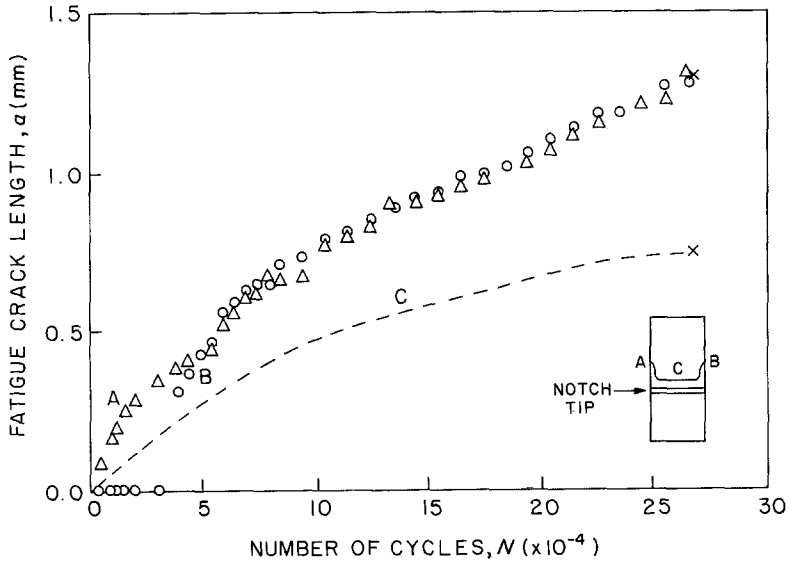


*Figure 4* A plot of the fatigue crack length against the number of cycles corresponding to the experiment shown in Fig. 3.

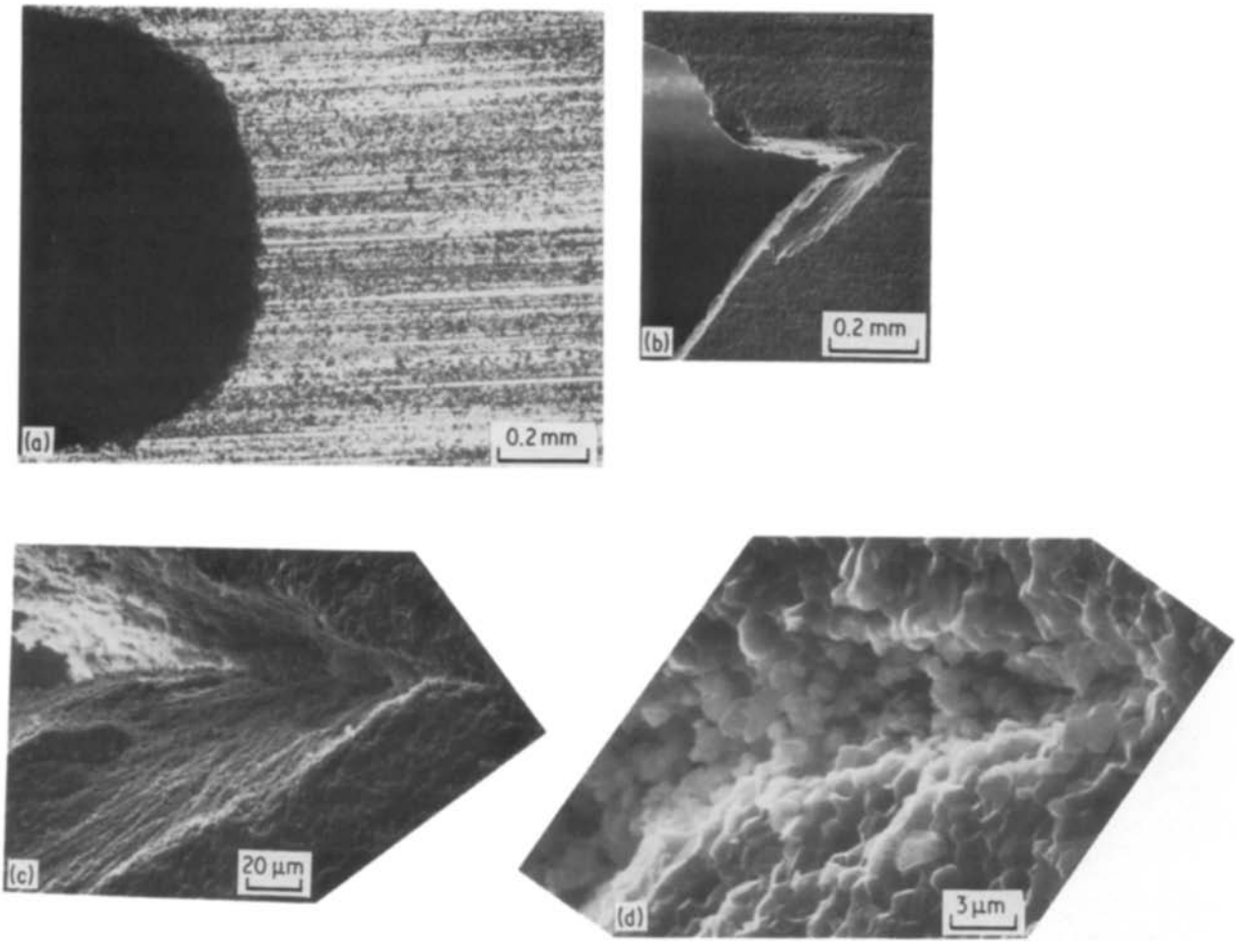


*Figure 5* (a) Profile of the notch subject to far-field cyclic compression in AD 999 in $Al_2O_3$; (b) fatigue crack at the notch-tip after 30 000 compression cycles; (c) and (d) higher magnification micrographs showing the details of intergranular fracture near the crack-tip.

In order to establish a basis for comparison with the failure mode observed in compression fatigue, a series of scanning electron micrographs of quasi-static (bend) fracture surfaces are provided in Fig. 8. The regions marked A and B in Fig. 8a are shown at a higher magnification in Figs 8b and c, respectively. This series of fractographs reveals: (i) within the generally intergranular fracture surface, there are islands of grains exhibiting cleavage facets, possibly as a result of the favourable orientation of the (crystallographic) cleavage planes to the local tensile stresses (Figs 8b and cd); (b) grain-boundary triple points are preferential sites for the nucleation of microcracks (Fig. 8c); (c) a grain separated by transgranular failure exhibits distinct cleavage patterns (e.g. Figs 8e and f), especially those containing microporosities at the grain interior/boundaries. The cleavage fracture mode was more prevalent in quasi-static fracture than during far-field cyclic compression. The morphologies of transgranular cleavage steps observed in Figs 7 and 8 are similar to those noted in the TEM replica studies of polycrystalline $Al_2O_3$ fractured in bending.

### 3.2. Oriented sapphire crystals

In order to compare with the results for polycrystalline ceramics, compression fatigue experiments were also performed in single crystals of $Al_2O_3$ where the plane of the notch was oriented along the $\{0\,0\,0\,1\}$ and $\{1\,\bar{2}\,1\,0\}$. In all these cases, application of the cyclic compressive load resulted in catastrophic fracture (splitting) parallel to the loading axis (Fig. 9a). There was no detectable stable crack advance (in Mode I) in either of these orientations. This result, in conjunction with the behaviour observed in polycrystalline $Al_2O_3$, suggests that grain boundaries in brittle ceramics play an important role in controlling the occurrence of Mode I crack growth observed under far-field cyclic compression. Microscopic observations on the fracture surfaces of single crystals reveal very clear traces of cleavage river patterns (Figs 9b and c).

### 3.3. Summary of results

On the basis of above experimental results and from repeated observations of crack growth in several experiments, the key characteristics of crack advance under far-field cyclic compression can be summarized as follows.

1. Cyclic compressive loads applied to notched specimens of polycrystalline ceramic materials result in (macroscopically) Mode I crack growth (Figs 2 and 3). The crack front is straight through the thickness of the specimen except within about 0.5 mm of the two side surfaces of the specimens, where the extent of damage is greater (Fig. 6a).

2. Cracks which initiate from the root of the notch propagate at a progressively decreasing velocity before arresting.

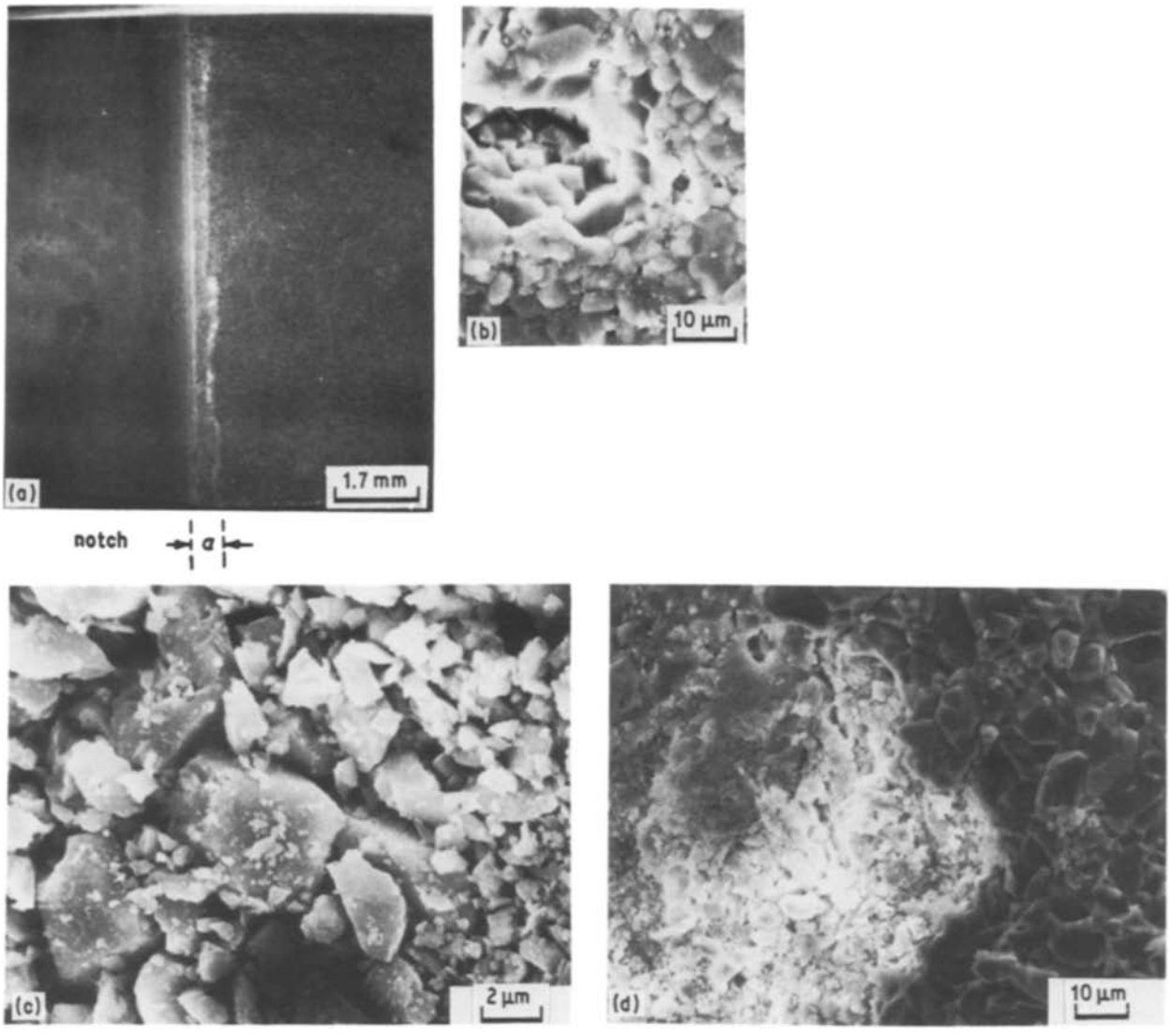


*Figure 6* (a) Micrograph of the fracture details of AD 995: fatigue fracture surface revealing a uniform crack front through the thickness of the specimen, $a$ refers to the fatigue crack growth distance; (b) crack-tip region showing intergranular fracture path; (c) intergranular fracture and debris formation observed on the fatigue fracture surface; (d) fractography showing the distinction between fatigue failure (on the left) and quasi-static (bend) fracture (on the right).

3. On the microscopic level, the mode of crack growth is primarily intergranular. Very sporadic traces of (transgranular) cleavage patterns are also observed (e.g. Fig. 7).

4. Intergranular crack advance under imposed cyclic compression results in the accumulation of debris particles within the growing crack.

5. The presence of such particles in the wake of the crack front leads to crack closure effects. (A detailed discussion of this mechanism is presented in a later

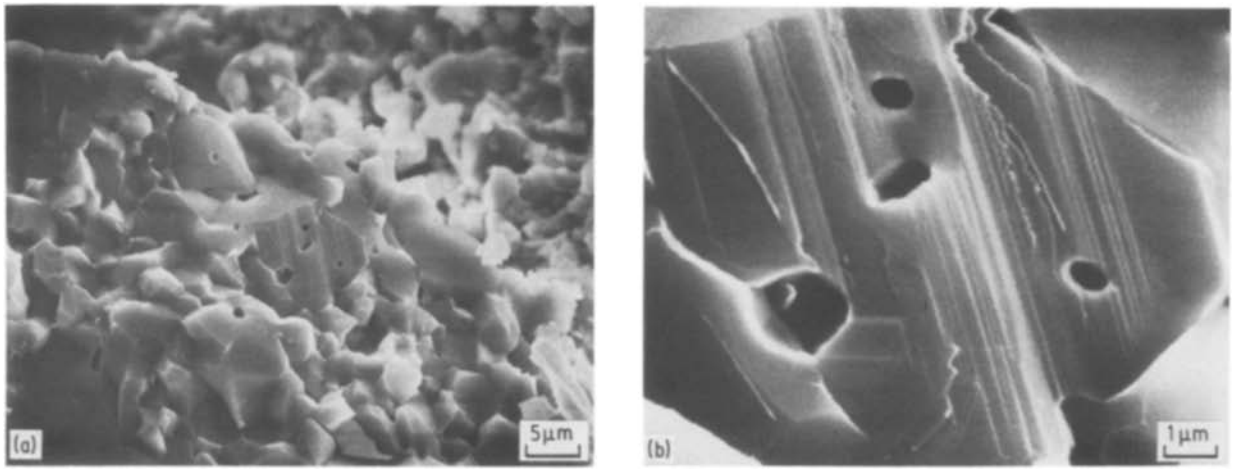


*Figure 7* (a) Intergranular fracture mode observed on the fatigue failure surface (without debris particles); (b) a higher magnification scanning electron micrograph of the central area in (a) showing transgranular cleavage fracture.

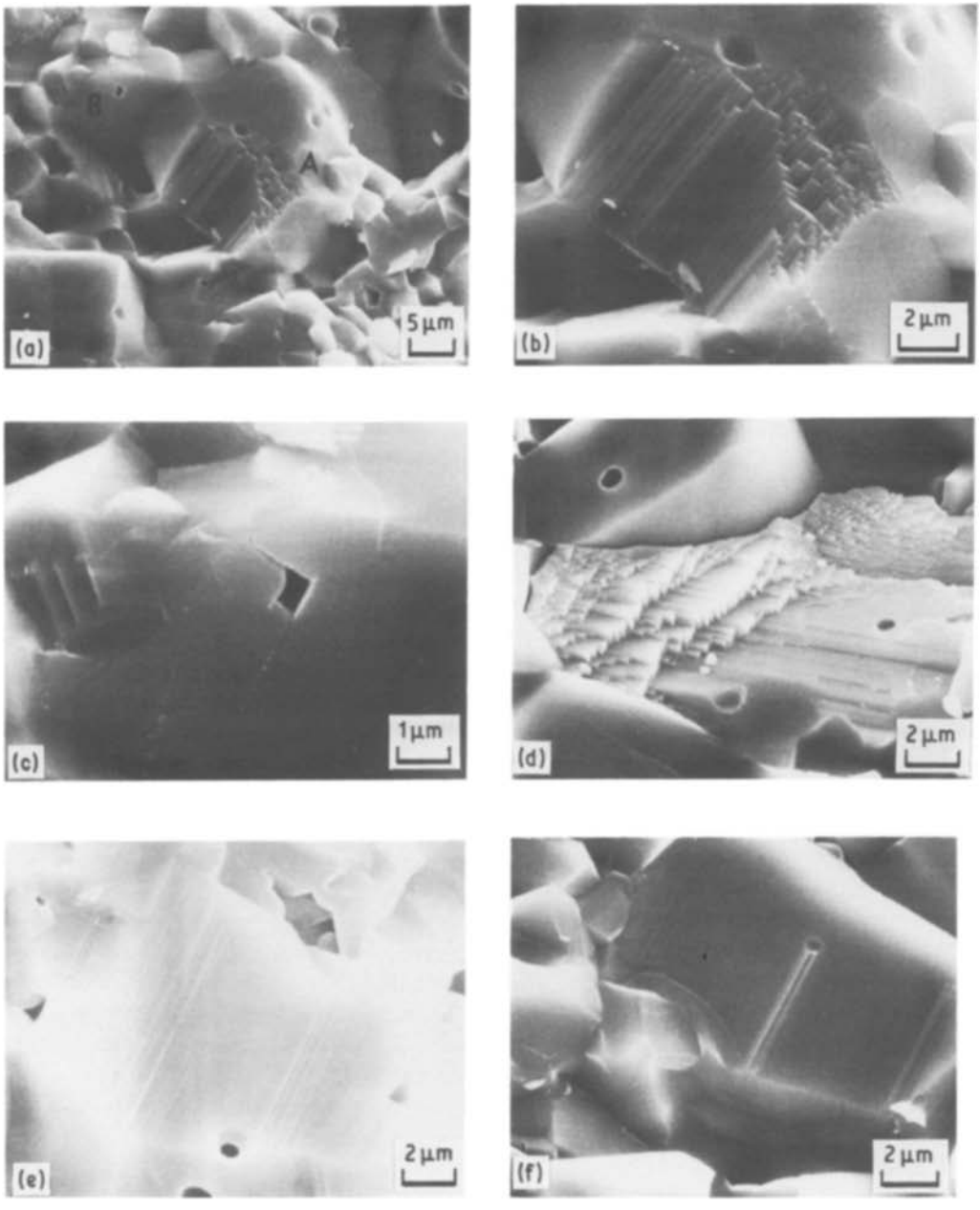


*Figure 8* (a) Quasi-static fracture surface of AD 995 $Al_2O_3$; (b) and (c) higher magnification micrographs of regions marked A and B, respectively, in (a); (d to f) transgranular cleavage failure modes.

section.) When the debris particles are periodically removed, the rate of crack advance is enhanced.

6. During part of the compression cycle, the region of residual tensile stresses within the damage zone at the tip of the advancing crack front is completely embedded in material elastically strained in compression. Furthermore, grain boundaries deflect the crack on a microscopic scale during cyclic failure. Therefore, stable and non-catastrophic cracking can occur even in brittle materials subject to far-field cyclic compression.

7. Grain boundaries play an important role in influencing crack growth behaviour under imposed cyclic compression. The application of cyclic compression loads to sapphire crystals results in a static mode (splitting) failure parallel to the loading axis, indicating that stable crack growth in ceramic materials may not occur at low temperatures in the absence of grain boundaries.

## 4. Discussion

The results presented in the previous section and those described earlier [11] appear to be the first systematic documentation of room-temperature fatigue crack propagation rates in ceramics under fully compressive cyclic loads. The occurrence of this phenomenon in metallic materials, however, has long been recognized (e.g. [13–17]). The fundamental mechanisms underlying crack propagation in ceramics are very different from those in metals as there is no macroscopic plasticity in the former class of materials at room temperature. Before discussing possible mechanisms of crack growth in ceramics subject to cyclic compression, we present a brief interpretative summary of recent advances in the understanding of this phenomenon in metals and alloys, to guide our comparisons with the behaviour of ceramics and to analyse the trends in ceramic-metal composites.


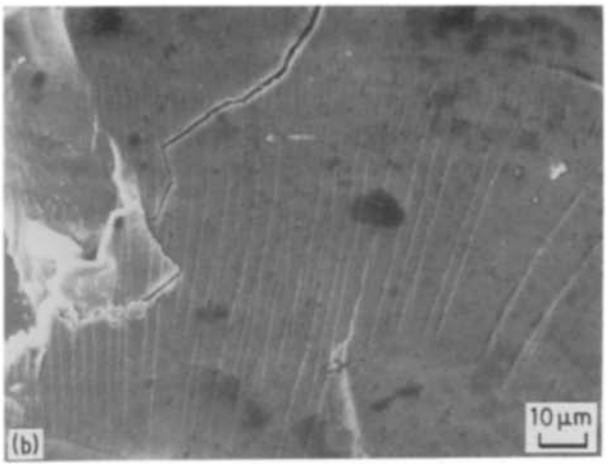


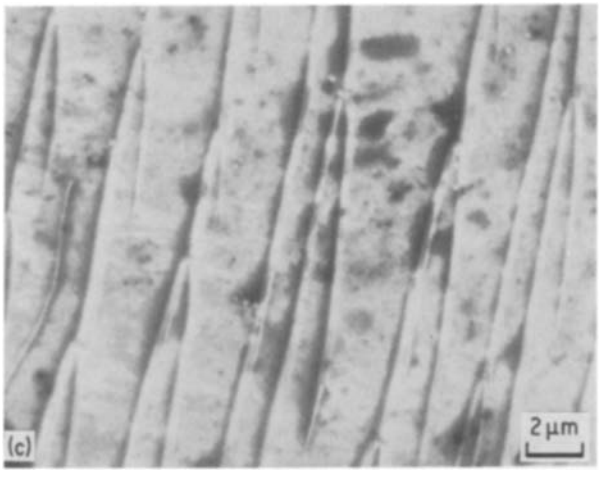


*Figure 9* (a) Splitting mode of fracture in a sapphire crystal where the plane of the notch is along the {0001} plane and the compression axis along the *c*-axis; (b, c) scanning electron fractographs revealing cleavage river patterns.

## 4.1. Metallic materials

A typical plot of the variation of fatigue crack length (measured from the notch-tip) as a function of the applied compression cycles generally observed in metallic alloys is illustrated schematically in Fig. 10a. The initially rapid rate of crack growth progressively decreases until complete crack arrest occurs. The principal factor responsible for the transgranular crack propagation under imposed compression in metals is the region of residual *tensile* stresses at the notch-tip created upon unloading from the maximum compressive stress [15]. The magnitude of the residual stresses and the size of the zone of residual tension ahead of a notch-tip subject to far-field cyclic compression can be estimated by analogy with the models for cyclic tension. In zero-tension fatigue, the removal of a tensile stress produces a region of residual compression at the tip of a crack as the elastically deformed material exerts a compressive stress on the plastic zone during the unloading process [18]. Fig. 10b schematically illustrates the variation of the normal stress ($\sigma_{yy}$) on the crack plane as a function of the distance ahead of the crack-tip ($x$) after the removal of a tensile load in an elastic-perfectly plastic material [18]. The region of residual compressive stresses, termed the reversed flow or cyclic plastic zone, is considered to be of a size $r_c$ where

$$r_c \approx \frac{1}{2\pi}\left(\frac{\Delta K_I}{2\sigma_0}\right)^2 \quad \text{in plane stress} \qquad (1a)$$

$$r_c \approx \frac{1}{6\pi}\left(\frac{\Delta K_I}{2\sigma_0}\right)^2 \quad \text{in plane strain} \qquad (1b)$$

$\sigma_0$ is the flow stress and $\Delta K_I$ the stress intensity factor

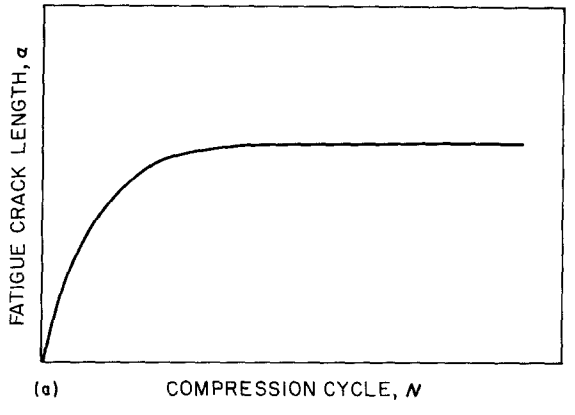


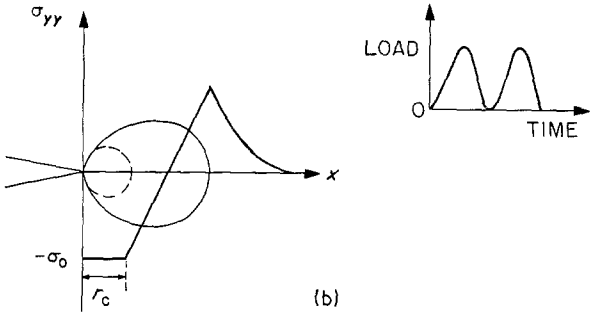


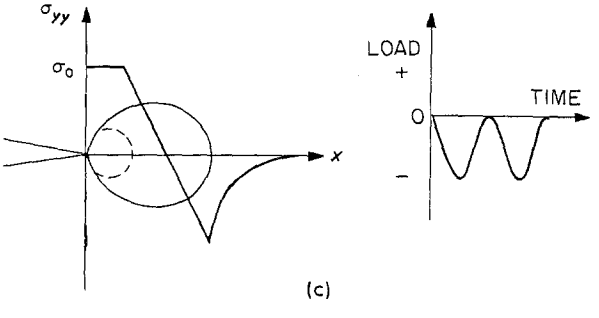


*Figure 10* (a) Typical crack growth behaviour in notched specimens of metallic materials subject to far-field cyclic compression; (b) schematic diagram showing monotonic and cyclic plastic zones at the tip of a crack loaded in cyclic tension; (c) region of residual tensile stress at the tip of a notch under far-field cyclic compression.

range, equal to the difference between the maximum and minimum values of the stress intensity factor, $K_{max}$ and $K_{min}$, respectively, during the *tensile* fatigue cycle. The size of the greatest prior plastic region (referred to as the monotonic or tensile plastic zone) is given by

$$r_y \approx \frac{1}{2\pi}\left(\frac{K_{max}}{\sigma_0}\right)^2 \quad \text{in plane stress} \qquad (2a)$$

$$r_y \approx \frac{1}{6\pi}\left(\frac{K_{max}}{\sigma_0}\right)^2 \quad \text{in plane strain} \qquad (2b)$$

By analogy with Fig. 10b, the variation of the normal stress with the distance ahead of the notch-tip can be schematically formulated for an elastic-perfectly plastic material subject to far-field cyclic compression (Fig. 10c). (Note, however, that Equations 1 and 2 may not be used directly to estimate the extent of notch-tip plasticity under far-field cyclic compression because of the changes in near-tip fields due to the notch angle and root radius and the occurrence of crack closure.) Equations 1 and 2 are applicable strictly for the case of a sharp tensile fatigue crack with no closure in its wake. Recently, Suresh and co-workers [15–17, 19] have carried out experimental and numerical studies of crack initiation and growth under far-field cyclic compression in metals. Such analyses provide parametric and quantitative predictions of the dependence of total crack growth distance under far-field cyclic compression on the applied load range, mechanical properties of the material, stress state and microstructure [15–17]. These studies have led to the following conclusions.

1. An increase in load range, at a fixed mean stress, leads to an increase in the total distance of crack advance under far-field cyclic compression [15–17].
2. Plane stress conditions promote a larger crack growth distance than plane strain [17].
3. The fraction of the loading cycle during which the crack is fully open progressively diminishes with increasing crack length; this fraction is larger for plane stress than for plane strain [17].
4. Effects of microstructure on crack growth in far-field cyclic compression are similar to those observed under cyclic tension because it is the local tensile stress which results in crack advance. However, microstructural effects on crack closure in tension–tension and compression–compression fatigue are significantly different [16, 19].
5. Whereas stable crack growth occurs from the notch-tip over hundreds of thousands of compression cycles, the amplitude of the very first compression stress cycle is found to have a decisive effect on the rate and total distance of crack advance under far-field cyclic compression. For example, a three-fold increase in the stress amplitude of the first compression cycle alone leads to about a ten-fold increase in the total distance of crack growth during the subsequent cycles.
6. The maximum amount of damage left at the tip of a crack grown (until arrest) under far-field cyclic compression in plane strain is not large enough to affect subsequent crack growth in tension–tension fatigue [16]. In view of this result, fatigue pre-cracking under far-field cyclic compression offers some unique possibilities for obtaining quick measurements of fatigue thresholds and ultra-low crack growth rates without the need for any artificial reductions in $\Delta K$ [15, 16].

## 4.2. Ceramic materials

The cyclic crack propagation behaviour in ceramics induced by compression fatigue loads (e.g. Figs 1 and 7) apparently resembles that observed in notched metallic materials (Fig. 10a). The mechanisms of fatigue in the two cases, however, arise from very different phenomena. Brittle solids such as ceramics, rocks, concrete or glass are known to fracture in monotonic compression in one of two mechanistically dissimilar patterns [13]:

1. In an *extrinsic* mode of fracture, large pre-existing cracks (of a size scale comparable to the dimensions of the component) extend under uniaxial or constrained compression in a direction roughly at right-angles to the shear plane. Here the displacement of the crack surfaces in shear provides the opening displacements at the crack tip sufficient to initiate an opening mode of failure. In this failure mode, cracks extend across planes of local maximum principal tension and curve in a direction parallel to the maximum principal axis of compression to result in the splitting of the part.
2. In an *intrinsic* mode of fracture, the accumulation of pre-existing microcracks or weak interfaces (of a size scale very much smaller than the dimensions of the component) results in a shear fault when a critical loading condition is met. Whereas the extrinsic fracture mode is a macroscopic process amenable to fracture mechanics characterization, the intrinsic fracture mode is a microscopic process which cannot be modelled accurately based on continuum principles alone. In the following section, we evaluate in detail the role of various mechanisms on cyclic fracture in ceramics.

### *4.2.1. Role of microplasticity*

Ceramic materials exhibit very little macroplasticity at room temperature, an apparent consequence of which is the poor ductility and fracture toughness in these brittle solids. There is, however, considerable controversy surrounding the role of *microplasticity* within the grain on low-temperature deformation in ceramics [20–25]. Heuer [20] has reported deformation twinning on rhombohedral planes in corundum ($\alpha$-$Al_2O_3$) crystals fractured in four-point bending at temperatures as low as $-196°C$. Based on studies of room-temperature (quasi-static) compression fracture in polycrystalline alumina, Rice [21] and Lankford [22] also suggest that microplasticity may play an important role in the failure of brittle solids. For example, the dependence of compressive strength on strain rate in $Al_2O_3$ has been regarded as an outcome of localized plasticity in the form of twinning, and possibly slip, where the microcracks are initiated at the point of intersection of the deformation bands with grain boundaries. Contrary to such interpretations, other researchers have proposed that plastic deformation by dislocation motion or twin formation and growth plays no role in the fracture process of

single-crystal and polycrystal ceramics at low temperatures [23, 25].

Our studies of cyclic crack propagation in both single-crystal and polycrystal $Al_2O_3$ indicate a predominantly brittle fracture process even on a microscale (e.g. Figs 5 to 9). While these observations alone are not sufficient to discard the possibility of microplasticity and its effects, in general, on mechanical properties of ceramics (which can only be verified through extensive high resolution microscopy studies), the role of microplasticity in governing stable crack growth under far-field cyclic compression does not appear significant on the basis of the following evidence: (i) the fracture mode in polycrystalline $Al_2O_3$ subject to cyclic compression is predominantly intergranular with no apparent trace of slip, (ii) cyclic compressive loads applied to oriented sapphire crystals produce catastrophic splitting parallel to the loading axis. The entire fracture surface is decorated with river patterns classically associated with intracrystalline cleavage (Figs 9b and c). The paucity of slip lines or twins is inconsistent with the arguments of plasticity effects at room temperature.

### 4.2.2. Role of stress corrosion cracking ("static fatigue")

As mentioned earlier, some researchers have suggested that cracking observed under cyclic loads may merely be an artefact of stress corrosion effects under certain temperature/loading conditions in ceramics [4–10]. For example, the tension fatigue results of Chen and Knapp [4] obtained for $Al_2O_3$ indicate a possible cyclic influence at room temperature, but no mechanical fatigue effect (over and above the stress corrosion effects) at temperatures greater than about 200° C. The fatigue crack growth behaviour observed in our work does not appear to be a manifestation of stress corrosion effects. Crack growth experiments performed *in vacuo* ($\leqslant 10^{-4}$ Pa pressure) show a definite mechanical fatigue effect under cyclic compression loads. Fig. 11 shows an example of a fatigue crack emanating from the notch-root in AD 995 $Al_2O_3$ subject to fully compressive cyclic loads *in vacuo*, the microscopic features of which resemble those observed in the laboratory environment.

### 4.2.3. Role of crack wedging by debris particles

A characteristic feature of crack advance under far-field cyclic compression is the formation of debris between the crack faces. An intuitive interpretation of the effect of such debris is that crack-tip opening is created under imposed compression by the wedging of the crack faces by hard particles. Although this wedging effect is likely to have some effect on Mode I crack advance, it is inconceivable that the extent of crack growth observed in ceramics under far-field cyclic compression can be attributed to crack wedging. In fact, experimental evidence appears to indicate that the presence of particles within the crack *reduces* crack growth in contradiction with intuitive expectations: (i) an increase in the length of the fatigue crack leads to an increase in the number of particles between the crack faces; however, crack growth rates are reduced with an increase in crack length (Fig. 1); (ii) periodic removal of the debris from within the crack increases crack propagation rates (Fig. 4); (ii) near the side

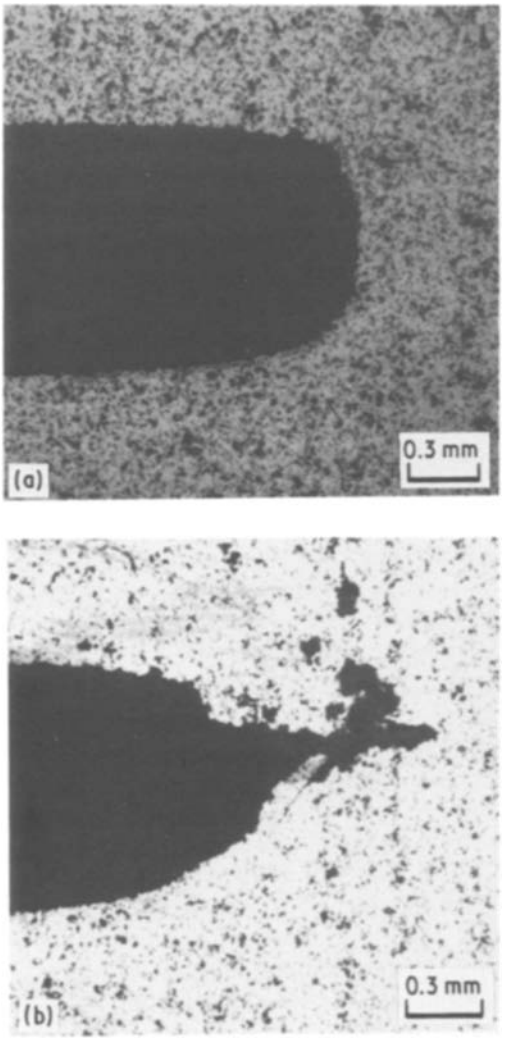


*Figure 11* (a, b, c) Optical micrographs showing the details of fracture under cyclic compression in AD 995 tested *in vacuo*.

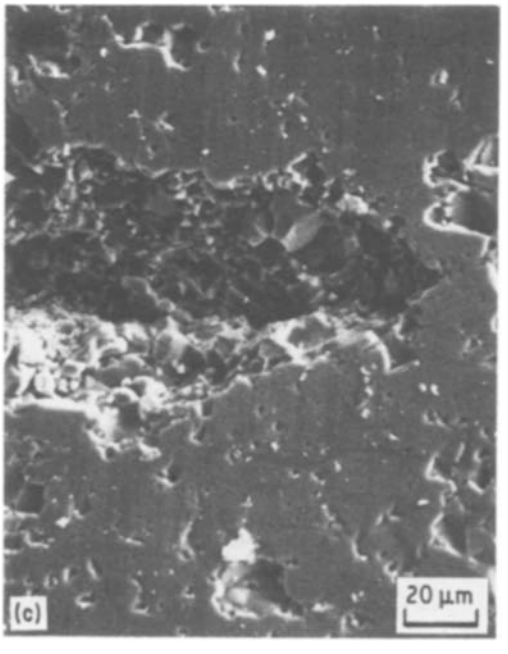

surfaces of the specimen, where the particles can easily escape from the crack during cyclic compression, the crack growth distance is larger than that observed in the centre-thickness section. Our results for polycrystalline ceramics, in concurrence with the tension fatigue behaviour documented for metals (e.g. [16]), reveal that debris particles accumulated between the crack faces reduce the effective driving force responsible for subsequent crack advance and promote crack closure.

### 4.2.4. Role of residual thermal stresses

In polycrystalline non-cubic ceramics with a random orientation of anisotropic grains, heating or cooling leads to a change in localized stresses across grain/phase boundaries [26–30]. The magnitude of the local stresses on a grain boundary depends on the change in temperature and the difference between the thermal expansion coefficients (and hence the relative crystallographic orientations of the adjoining grains/phases). At high temperatures, thermal contraction mismatch can be relaxed by diffusional creep [30]. It has been suggested [26] that there is a critical temperature $T_f$ below which stress relaxation ceases and the residual stresses increase linearly with

$$\Delta T = T_f - T_{ambient} \quad (3)$$

$T_f$ is a function of the grain size and cooling rate. The calculation of thermal residual stresses on a grain boundary in a polycrystalline solid comprising randomly oriented crystals is a problem not amenable to a straightforward theoretical formulation. Highly simplified models have been proposed in the past [26, 29, 31]; a common feature of such models is that the most prevalent residual stresses take the form

$$\sigma_{ij} \sim \tilde{f} \frac{E\Delta\alpha\,\Delta T}{(1+\nu)} \quad (4)$$

Here $E$ is the elastic modulus, $\nu$ the Poisson ratio, $\Delta\alpha$ the difference in thermal expansion coefficients of the grains on either side of the boundary, $\tilde{f}$ is a function of the crystallographic orientations of the grains contributing to the residual stress on the boundary and of the distance from grain triple points and microvoids. Experiments reveal that such residual stresses are not significant in cubic crystals and that the elastic anisotropy can be considered negligible in comparison with thermal contraction anisotropy. Residual stresses induced by mismatch between grains are known to play a decisive role in the fracture of ceramics. The existence of such internal stresses alone is not the cause of fatigue failure since high-frequency cyclic compressive stresses (of magnitude $\sim 300$ MPa) are required to induce measurable cracking over tens of thousands of fatigue cycles. The role of residual stresses in fracture under far-field cyclic compression is examined in a later section in conjunction with other mechanistic processes.

## 4.3. Micromechanics of failure

The results of our investigation guide us to formulate the following line of reasoning which models key elements of cyclic fracture under far-field compression in ceramics. We begin with a continuum analysis of damage at the notch root, and subsequently examine the micromechanics of crack growth.

### 4.3.1. Notch-tip process zone

In notched specimens loaded in uniaxial compression, the material elements in the vicinity of the notch-tip are subject to locally elevated stress levels. Stress intensification at the notch-tip can be conveniently analysed using linear elastic fracture mechanics [32]. Consider a slender notch of root radius, $\varrho$ (Fig. 12a). Along the notch plane, the variation of the normal stress $\sigma_{yy}$ with distance $r$ ahead of the notch-tip is given [32] by

$$\sigma_{yy} = \frac{K_I}{(2\pi r)^{1/2}} \frac{\varrho}{2r} + \frac{K_I}{(2\pi r)^{1/2}} + \sigma^\infty \quad (5)$$

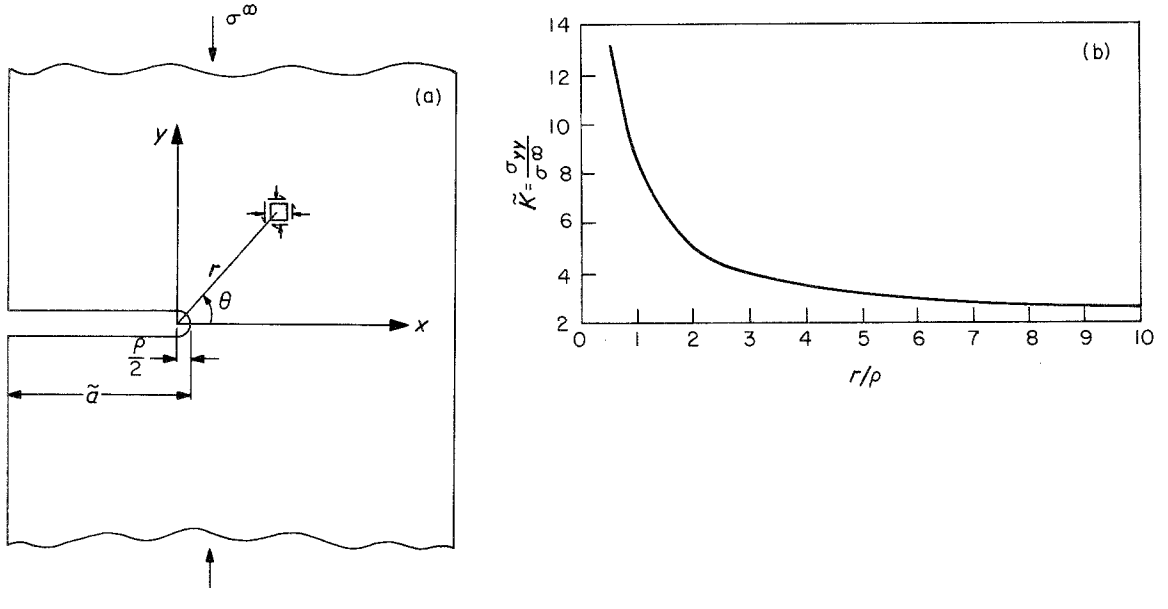


*Figure 12* (a) Nomenclature for the geometry of a slender notch in an infinite plate loaded in compression; (b) variation of non-dimensional stress $\sigma_{yy}/\sigma^\infty$ on the plane of the notch as a function of non-dimensional distance $r/\varrho$.

The stress intensity factor $K_I$ is

$$K_I = \sigma^{\infty}(\pi\tilde{a})^{1/2}F \quad (6)$$

where $F$ is a constant dependent upon the specimen geometry and notch length, $\tilde{a}$ ($F = 2.1$ for the polycrystalline $Al_2O_3$ specimen). Combining Equations 5 and 6,

$$\tilde{K} = \frac{\sigma_{yy}}{\sigma^{\infty}} = \frac{F\varrho}{2r}\left(\frac{\tilde{a}}{2r}\right)^{1/2} + F\left(\frac{\tilde{a}}{2r}\right)^{1/2} + 1 \quad (7)$$

This equation, plotted in Fig. 12b, gives an indication of the stress intensification due to the presence of the notch, as a function of the distance ahead of the notch-tip. ($F$, $\varrho$ and $\tilde{a}$ are known parameters.) The extent of damage (i.e. microcracking) induced by the (maximum) compressive stress $\sigma^{\infty}_{min}$ can be determined accurately only on the basis of the *local* stress state at the grain boundary. However, an estimate of this damage zone, at a continuum level, can be achieved by assuming that the process zone size $r_c$ is the distance ahead of the notch-tip over which the normal stress $\sigma_{yy}$ exceeds a critical value, $\sigma_{cr}$. If $\sigma_{cr}$ is set equal to the unconstrained compressive strength of the AD 995 material ($\simeq 2620$ MPa), $r_c = 0.24$ mm ($r$ is measured from the origin located at a distance $\varrho/2$ behind the notch-tip; Fig. 12). We emphasize that this is only a first-order estimate of the extent of damage induced by the first compressive cycle, because the compressive strength of brittle solids is known to be strongly dependent upon constraint (triaxiality).* A refined calculation of the damage zone size should include experimental measurements of compressive strength under triaxial stress conditions which are similar to those at the tip of the notch.

The nucleation of microcracks need not necessarily lead to the formation of a macrocrack over this entire distance because (i) grain-boundary residual stresses arising from thermal contraction anisotropy are alternatingly tensile and compressive in nature, and (ii) there is a strong stress gradient ahead of the notch. The coalescence of microcracks along the grain boundaries occurs progressively during the subsequent compressive cycles under the influence of the local stresses prevalent at grain boundaries. The initially rapid rate of growth (over a distance of about 0.3 to 0.5 mm as shown by the data sets A and B in Fig. 1 and Curve C in Fig. 4) is consistent with the above calculations of a distance of microcracking and damage influenced by the first compression cycle. Comprehensive numerical and experimental studies in metals also show that the total crack growth distance under far-field cyclic compression is very strongly influenced by the maximum compressive stress imposed prior to the nucleation of a fatigue crack from the notch-root [19]. Although the mechanisms of crack growth in metals are different, this line of reasoning is in accord with the general inference that the decisive role of the initial compression cycle in determining the maximum extent of damage at the notch-tip is a characteristic feature of crack growth under far-field compression fatigue. Also the observations of a longer crack growth distance at the two side surfaces, as compared to the specimen interior, are consistent with the well-known result that the compressive strength of brittle solids is increased by constraint.

### 4.3.2. Tensile residual stresses at the notch-tip

Experimental observations of the side surfaces of polycrystalline ceramics and ceramic–metal composites reveal the existence of microcracks at the notch-tip upon unloading from a static compressive stress. Given the possibility of irreversible sliding of cracked grain facets during far-field compression and the accomodation of such displacements by adjacent grains, it is conceivable that a fraction of the grain-boundary microcracks (nucleated during the compressive loading cycle) can remain open during the unloading portion of the fatigue cycle. The opening of a population of grain-boundary microcracks within the process zone at the notch-tip leads to a reduction in the elastic modulus of the material in the (microcracked) process zone. This zone of damage is shielded from the far-field cyclic compressive stress by material elastically strained in compression. The differential in the compliance of the material within the process zone and that of the surrounding material can then induce residual *tensile* stresses during unloading from the maximum compressive condition over a distance of the order of the size of the process zone.

Fig. 13 is a schematic diagram of the constitutive behaviour, describing possible non-linear stress/strain characteristics of a brittle solid cycled in compression. The non-linear behaviour (Curve A), initiated at some critical compressive stress, can be induced by microcracking, phase transformation, plasticity or viscous deformation, in general. Upon unloading from the maximum compressive stress, the stress–strain behaviour follows Curve B in Fig. 13 if no permanent displacements exist. Physically, this corresponds to a

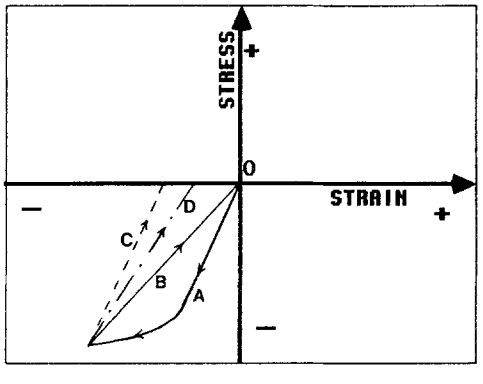


*Figure 13* An idealized schematic diagram of possible variations in constitutive behaviour of a microcracking medium stressed in cyclic compression. Curve A represents the non-linear stress–strain curve due to the onset of microcracking; Curve B denotes unloading to the origin when all microcracks are fully closed; Curve C represents unloading parallel to the initial slope of Curve A. Curve D represents the intermediate situation.

*Note, however, that even large differences in the compressive strength lead only to small changes in the damage zone size, $r_c$, because of the steep gradient in the $\sigma_{yy}/\sigma^{\infty}$ against $r/\varrho$ plot near the notch-tip (Fig. 12b).

situation where the microcracks created within the notch-tip "process" zone during the application of a compressive load fully close upon removal of the compressive stress. On the other hand, if a number of microcracks are prevented from complete closure because of friction or the presence of debris particles during the unloading portion of the compressive cycle (where the constitutive response is represented by the dotted line C in Fig. 13), residual *tensile* stresses are created at the notch-tip. The dotted line C is parallel to the initial portion of the loading line A. Curve D represents an intermediate situation where partial opening of the microcracks is observed. Brockenbrough and Suresh [33] have recently conducted a finite-element simulation of microcracking in notched plates of polycrystalline ceramics stressed under cyclic compression (see Appendix for details). Their results do corroborate the existence of a zone of residual tension at the notch-tip when even a small fraction of the total number of microcracks does not close during the unloading portion of the compression cycle. Similarly, if phase transformations occur at the notch-tip during compression loading and permanent strains exist upon unloading from the far-field compressive stress, residual *tensile* stresses will be induced at the notch-tip. It is this residual tensile stress field which appears to be the principal factor contributing to the growth of Mode I fatigue cracks in ceramics loaded in uniaxial cyclic compression.

### 4.3.3. Frictional sliding and opening of microcracks

Continuum analysis of a damage zone provides only a partial description of the failure process because the overall fatigue effect is dictated by the micromechanics of grain-boundary fracture. The nominal far-field compressive stress $\sigma^\infty$ produces a normal stress $\sigma_n$ and a shear stress $\tau_n$ on a grain boundary oriented at an angle $\alpha$ to the compression axis (see the schematic diagram in Fig. 14).

$$\sigma_n = \sigma^\infty \sin^2 \alpha \tag{8a}$$

$$\tau_n = \sigma^\infty \sin \alpha \cos \alpha \tag{8b}$$

Note that the far-field compressive stress is

$$\sigma^\infty = \left(\frac{\sigma^\infty_{max} + \sigma^\infty_{min}}{2}\right) + \left(\frac{\sigma^\infty_{max} - \sigma^\infty_{min}}{2}\right) \sin 2\pi \nu t \tag{9}$$

where $\nu$ is the frequency of fatigue loading and $t$, the time.

The rate-limiting step for the initiation of a *macrocrack* from the notch-tip is the coalesence of microcracks along the grain boundaries. In this context, it is

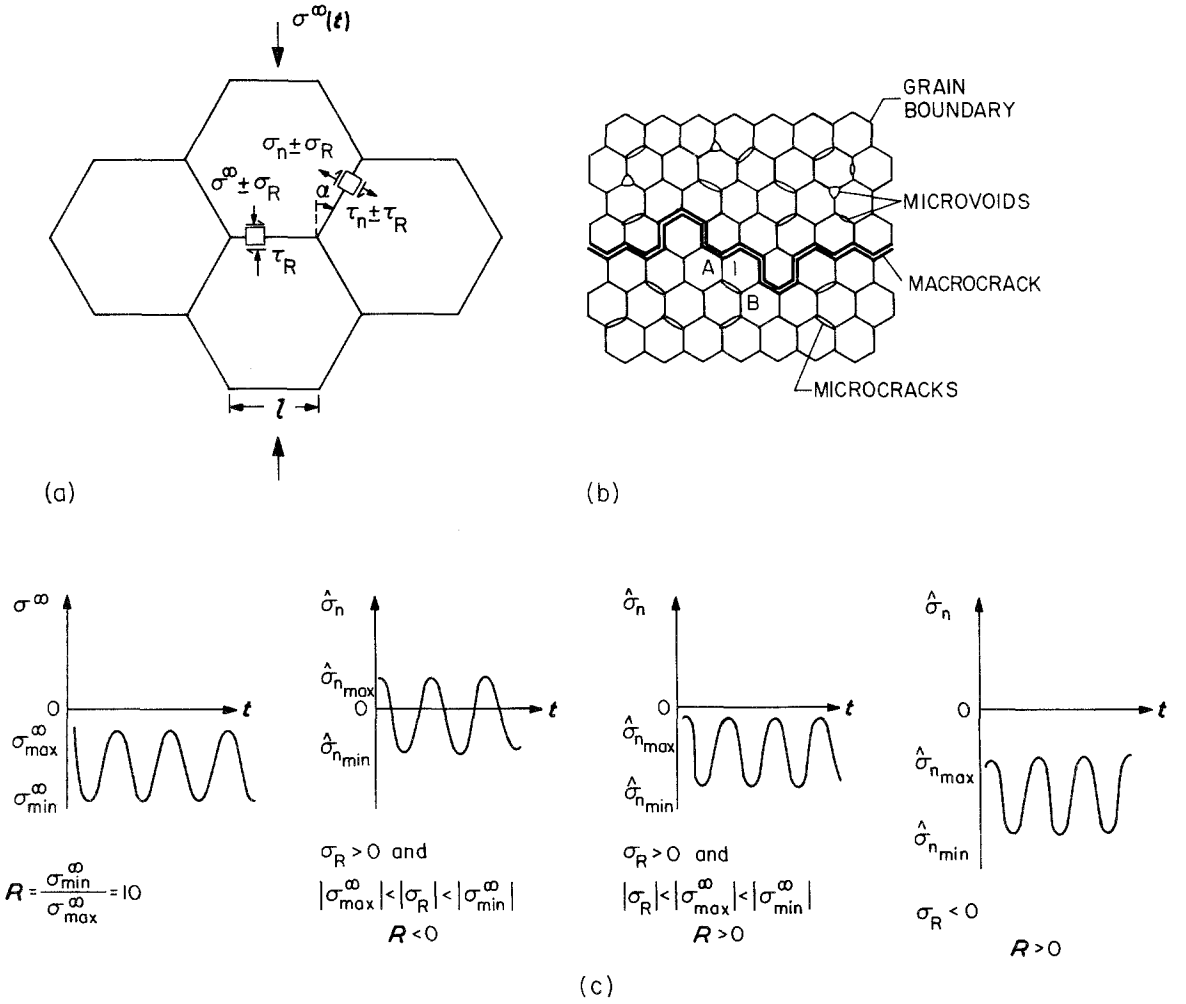


*Figure 14* (a) Schematic diagram showing stresses on grain boundary due to far-field compression and residual stresses caused by anisotropic contraction of nearby grains; (b) schematic diagram showing microvoids on grain facets and triple points, grain boundary microcracks and macrocrack growth through intergranular separation; (c) various possibilities for loading patterns on a grain boundary for a given far-field fatigue cycle of $R = 10$.

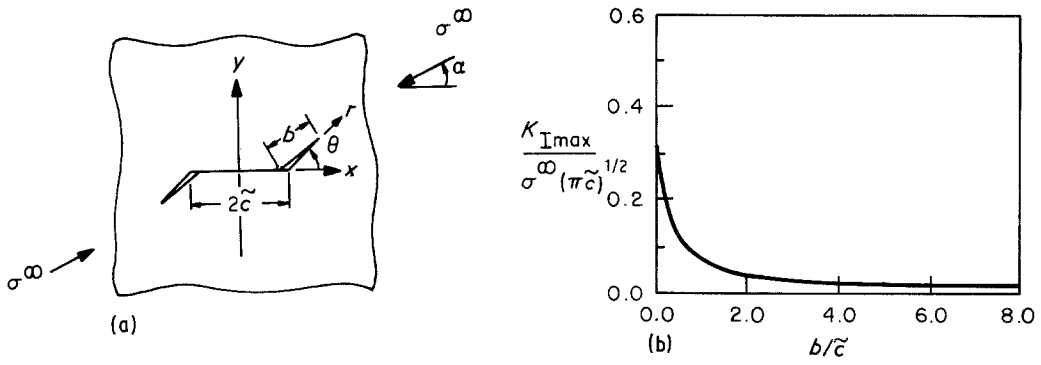


*Figure 15* Closed microcrack oriented at angle $\alpha$ to the far-field compression axis and its compression-induced kink extends at an angle $\theta$; (b) variation of maximum $K_I$ with the kink length $b$ under uniaxial far-field compression $\tau_c = 0$ and $\mu = 0.3$ [35].

instructive to consider the various theories defining the conditions for the growth of microcracks in brittle solids loaded in uniaxial quasi-static compression. In the well known Griffith approach, it is believed that fracture occurs when the local tensile stress exceeds the cohesive strength of the material (see [34] for a detailed discussion). McClintock and Walsh [34] modified the Griffith fracture criterion to include frictional effects that may accompany crack closure under compression. During uniaxial compression of plates of brittle materials containing pre-existing flaws oriented at a certain angle to the compression axis, the relative frictional sliding of the faces of the pre-existing cracks may produce, at their tips, tension cracks which deviate sharply from the sliding plane. Nemat-Nasser and Horii [35] have shown that a suitably oriented pre-existing crack first kinks at an angle of about $0.4\pi$ relative to its initial straight direction and then curves into a position parallel to the maximum axial compressive force. Near the tip of the initial crack of length $2\tilde{c}$ (see Fig. 15) and prior to kinking,

$$\sigma_{\theta\theta} = \frac{3}{4}\frac{k_2}{(2\pi r)^{1/2}}\left(\sin\frac{\theta}{2} + \sin\frac{3\theta}{2}\right) \quad (10a)$$

where $k_2$ is the Mode II stress intensity factor at the initial crack tip defined by

$$k_2 = \tau^*(\pi\tilde{c})^{1/2} \quad (10b)$$

$$\tau^* = \tau_{xy} + \tau_c - \mu\sigma_y \quad (10c)$$

$$= \tfrac{1}{2}\sigma^{\infty}\sin 2\alpha + \tau_c - \mu(\tfrac{1}{2}\sigma^{\infty} - \tfrac{1}{2}\sigma^{\infty}\cos 2\alpha) \quad (10d)$$

The parameters in the above equations, also shown in Fig. 15, are: $\sigma_y$ and $\tau_{xy}$, the normal and shear stresses on the pre-existing crack, respectively; $\alpha$, the inclination of initial flaw to the compression axis; $\mu$, the coefficient of friction between the crack faces; and $\tau_c$, the cohesive strength. The Mode I stress intensity factor $k_{1\theta}$ at the tip of a very small kink emanating at an angle $\theta$ from the initial crack is

$$k_{1\theta} = -\tfrac{3}{4}k_2\left(\sin\frac{\theta}{2} + \sin\frac{3\theta}{2}\right) \quad (11)$$

Maximization of $k_{1\theta}$ with respect to $\theta$ yields the critical angle of $\theta_c = 0.392\pi$ [35]. For uniaxial compression, the variation of the maximum (local) tensile opening stress intensity factor with the kink length, $b/l$, is shown in Fig. 14 for $\mu = 0.3$ and $\tau_c = 0$. The most significant outcome of this figure is the result that a kink propagating from an initial crack oriented at angle $\alpha$ to the uniaxial compression axis experiences a monotonically diminishing opening stress intensity $k_{1\theta}$ at its tip. Thus, crack growth from an initial flaw is stable and non-catastrophic under uniaxial compression for the conditions indicated.

Although the above continuum solutions are not directly applicable to the microfracture process under consideration, they provide a physically-appealing rationale for the stability of the cyclic crack growth process under imposed compressive stresses. In the present context, it is reasonable to suppose that a microcrack will propagate along an adjacent grain-boundary facet with an orientation $\theta$ which provides the highest $k_{1\theta}$ in Equation 11 among the facets in its vicinity. This kinked crack may not propagate into a third boundary because (a) the residual (normal) stresses on that boundary may be compressive; (b) the microcrack has to change its orientation to advance into the adjacent boundary. This leads to a reduction in the (near-tip) "driving force" due to crack kinking (Fig. 14); (c) the grains in the vicinity of a cracked boundary may be too small to permit a preferential fracture path. There is some evidence in our study that fracture may occur preferentially along the boundaries of larger grains (e.g. Fig. 6b). It is also known from prior work that there is a critical grain size $l^*$ below which the residual stresses produced by differential thermal contraction are not large enough to nucleate microcracks (e.g. [31]). (Note, however, that the shear stresses exerted on the grain boundary by the far-field compressive load can induce microcracking even if the grain size is smaller than $l^*$.)

### 4.3.4. Predictions and comparisons with experiments

The implications of the above analyses can be appreciated through the following model calculations. For the fatigue results outlined in Fig. 1, $\sigma^{\infty}_{\max} = -29.8$ MPa and $\sigma^{\infty}_{\min} = -298$ MPa. A grain-boundary microcrack oriented at an average angle $\alpha = 45°$ to the compression axis would experience a shear stress $\tau^* = -105$ MPa (Equation 10d) for $\tau_c = 0$ and $\mu = 0.3$. If the microcrack is located in the vicinity of the notch-tip ($\varrho/2 < r < \varrho$ in Fig. 12), $\tau^*$ would be amplified by the stress concentration of the notch $\tilde{K}$ (Equation 7). A grain boundary oriented at $\theta = 60°$ with respect to the microcrack (in the hexagonal grain

model) will experience a Mode I stress intensity $k_{1\theta} \approx$ 2.6 to 3.6 MPa $m^{1/2}$ (Equations 10 and 11) for $\tilde{K} = 5$ to 10 and average facet length $2\tilde{c} = 8\,\mu m$. One finds that $k_{1\infty} \sim K_c$, the (grain boundary) fracture toughness ($\sim$2 to 4 MPa $m^{1/2}$ for $Al_2O_3$ of grain size $\approx 20\,\mu m$ and average (intergranular fracture energy $\gamma \approx$ 10 to 20 J $m^{-2}$ where $\gamma = K_c^2/2E$ [27, 31]). Another way to examine the same process is to calculate the $\tilde{K}$ which is needed to make $k_{1\theta} = K_c$. For the above conditions and for $K_c = 2$ MPa $m^{1/2}$ this value of $\tilde{K} = 4.78$. From Fig. 12b, we note that $\tilde{K} > 4.78$ over a distance $r/\varrho = 2$ or 1 mm ahead of notch-tip. For $K_c = 4$ MPa $m^{1/2}$, this distance is about 0.4 mm. In the above calculations, an average value of $\alpha = 45°$ was used. However, even if one considers a range of $\alpha = 30$ to 60°, the predicted values of $k_{1\theta}$ would still be within the acceptable limits of $K_c$. These predictions clearly indicate that the maximum magnitude of the far-field compressive stress $\sigma^\infty$ in our experiments is large enough to induce a damage zone at the notch-tip and is capable of producing subsequent crack growth over a distance of about 0.5 to 0.75 mm (Fig. 1).

The fatigue crack advances by the coalescence of microcracks once the far-field cyclic compressive stresses create a sufficient microcrack population in the vicinity of the current crack-tip. Preferential crack advance along the larger grain boundaries is likely to be a cause for the formation of large debris particles during crack growth. As the fatigue crack advances, debris particles accumulate within the crack faces. (For example, if the grain facets A and B in Fig. 14b fracture during the compressive cycle, the grain (marked 1) will be removed from the surface and would form a wedge between the crack facets.) The consequent build-up crack closure (which has been studied extensively in metallic materials (e.g. [15–17]) leads to a progressive reduction in growth rates. The crack growth process under far-field cyclic compression is always non-catastrophic because the local zone of damage at the tip of the macroscopic crack is always encompassed by material elastically loaded in compression. Furthermore, the deflection of the crack at grain boundaries leads to a reduction in the "effective driving force" and stabilizes crack advance.

The results discussed earlier provide a variety of circumstantial evidence supporting the above model descriptions of the possible mechanisms of cyclic crack advance. Furthermore, the occurrence of stable, non-catastrophic fracture even in brittle $Al_2O_3$ at room temperature is consistent with the characteristic feature of internal stresses; microcracking in a residual stress field is an intrinsically stable process because the residual stress field is alternatingly tensile and compressive in nature.

### 4.3.5. Residual stresses due to differential thermal mismatch

In a polycrystalline ceramic with a random orientation of grains, the grain boundaries are subject to a *net* normal stress

$$\hat{\sigma}_n = (\sigma_n + \sigma_R) = (\sigma^\infty \sin^2\alpha + \sigma_R) \quad (12a)$$

and a net shear stress

$$\hat{\tau} = (\tau_n \pm \tau_R) = (\sigma^\infty \sin\alpha \cos\alpha \pm \tau_R) \quad (12b)$$

Here $\sigma_R = \sigma_{22}$ and $\tau_R = \sigma_{12}$ in Equation 4. Note that $\sigma_n$ is compresive whereas $\sigma_R$ can be tensile or compressive depending upon the crystallographic orientations of the grains contributing to the residual stress on a grain boundary in this two-dimensional model (Fig. 14a). If the grain boundaries are located in the vicinity of the notch-tip, the stresses $\hat{\sigma}_n$ and $\hat{\tau}$ are enhanced by the stress concentration of the notch (Equation 7). Furthermore, microvoids located at grain triple points and grain boundaries increase the magnitude of the local stresses (Fig. 14b). Thus, the actual density of microcracks nucleated during the early compression cycles is determined by $\hat{\sigma}_n$ and $\hat{\tau}$ suitably modified to account for the *local* stress intensification. At the maximum load of the fatigue cycle,

$$\hat{\sigma}_{n_{max}} = \sigma^\infty_{max} \sin^2\alpha + \sigma_R \quad (13a)$$

$$\hat{\tau}_{max} = \sigma^\infty_{max} \sin\alpha \cos\alpha + \tau_R \quad (13b)$$

At the minimum load of the fatigue cycle

$$\hat{\sigma}_{n_{min}} = R\sigma^\infty_{max} \sin^2\alpha + \sigma_R \quad (14a)$$

$$\hat{\tau}_{min} = R\sigma^\infty_{max} \sin\alpha \cos\alpha + \tau_R \quad (14b)$$

where $R$ is the load ratio ($= \sigma^\infty_{min}/\sigma^\infty_{max}$). Different possibilities for the amplitude of $\hat{\sigma}_n$ on a grain boundary are illustrated in Fig. 14c for various values of $\sigma_R$, $\sigma^\infty$ and $\alpha$. The shear stress $\hat{\tau}$ also follows similar trends.

Consider now the possible role of residual stresses on uncracked grain boundaries. Although the quantification of residual stresses is a complex problem and is beyond the scope of this paper, one may attempt an order-of-magnitude approximation to illustrate their importance in fracture. Taking values of $E =$ 372 GPa, $\nu = 0.22$, $\Delta T = 1500°$C and $\Delta\alpha = 3.7 \times 10^{-7}(°\,C)^{-1}$ for $Al_2O_3$ [31] and setting $\tilde{f} = 1$ in Equation 4, the theoretical maximum value the residual tensile stress is found to be $\sigma_R \approx 170$ MPa. (The conditions for maximum $\sigma_R$ are favoured in h c p structures when the $c$-axis of one grain is perpendicular to the grain boundary and the $c$-axis of the adjacent grain is parallel to the boundary [30].) Experimental measurements of residual stresses are very complicated and are prone to considerable uncertainties. It is, however, interesting to note from the work of Blendall and Coble [30] that a direct method of measuring residual stresses through broadening of spectroscopic R lines (692 and 69 nm, due to $Cr^{3+}$ impurities) provided the value of maximum residual stress $\sigma_R \sim 120$ MPa for coarse-grained (grain size $\geqslant 50\,\mu m$) $Al_2O_3$, which is in reasonable concurrence with Equation 4. An uncracked grain boundary oriented at an (average) angle $\alpha = 45°$ to the compression axis would be subjected to a maximum and minimum normal stress $\hat{\sigma}_{max} \approx 105$ MPa and $\hat{\sigma}_{min} \approx -29$ MPa during the fatigue cycle (from Equations 13a and 14a) for $\sigma_R = \tau_R \sim 120$ MPa). Furthermore, the magnitude of the shear stresses on this boundary under the influence of far-field compression would oscillate between $\hat{\tau}_{max} = -135$ MPa and $\hat{\tau}_{min} = -300$ MPa (Equations 13b and 14b). These calculations illustrate that the residual stresses

caused by thermal contraction anisotropy, in conjunction with the far-field compressive loads, can impose large shear stresses on grain facets. Furthermore, thermal contraction anisotropy can induce large tensile stresses on some grain boundaries. A criterion for grain-boundary failure based on the above mechanism cannot be formulated at this time in view of the lack of reliable and reproducible measurements of thermal residual stresses. In order to isolate from other mechanisms the contribution to fatigue from thermal contraction anisotropy, and to compare with the results of this study, we are currently examining the effect of far-field cyclic compression on crack growth in cubic systems where residual stresses from thermal expansion differences between grains are known to be relatively insignificant.

#### *4.3.6. Some outstanding issues*

The results, analyses and interpretative discussions presented in earlier sections have enabled the identification of several key mechanisms controlling crack advance in ceramics under cyclic compression. There are, however, several aspects of this problem which warrant extensive further investigation. Firstly, the mechanisms underlying microcrack coalesence and the resultant growth of a macroscopic Mode I fatigue flaw are not clearly understood at this time. Further work is needed to elucidate the effects of cyclic frequency and mean stress on the mechanics of microcrack coalesence so that the observed growth rates under far-feld cyclic compression (for a given material and loading conditions) can be theoretically justified. Secondly, experiments in well controlled "model" microstructures are necessary to identify the role of grain-boundary (glassy) phases and grain size in the fracture of ceramics under applied compression fatigue loads. Thirdly, extensive research is needed to study the mechanisms of cyclic crack growth in ceramics subjected to compressive stresses under the more realistic conditions of elevated temperatures where diffusional creep and grain-boundary sliding are important. Fourthly, careful experimental work should be undertaken in cubic and non-cubic ceramic systems to isolate the contributions to compression fatigue fracture from residual stresses induced by thermal contraction mismatch between grains in polycrystalline ceramics.

### 4.4. Ceramic–metal composites

In ceramic–metal composites, such as cemented carbides, the application of far-field cyclic compressive loads can result in fatigue crack growth from notches by a combination of the mechanisms discussed for metals and ceramics: (i) residual tensile stresses induced by cyclic plasticity in the metallic binder and by the non-closure of microcracks at the carbide–binder interface during compression fatigue; (ii) residual tensile and shear stresses present at the carbide–binder interface due to differential thermal contraction effects; and (iii) frictional sliding of interfacial microcracks due to far-field compressive loads.

The thermal mismatch effect is an especially significant factor for cemented carbides because of the large differences in the thermal expansion coefficients of the carbide and the metallic binder. Consider, for example, a WC–Co composite material. On an average, the difference between coefficients of thermal expansion for WC and cobalt is $\Delta\alpha \sim 10^{-5}(^\circ C)^{-1}$ and no significant stress relief occurs below $\sim 800^\circ C$. Therefore, the average residual strain at the WC–Co interface due to differential thermal contraction is $\Delta\varepsilon = \Delta\alpha\Delta T \approx 8 \times 10^{-3}$. Recent work by Suresh and Sylva [12] on WC–25 wt % Co composites has shown that stable room-temperature fatigue crack propagation in cyclic compression can occur over distances of the order of 1 mm. The variation of crack length with the number of compression cycles is similar to that observed in Fig. 1 for $Al_2O_3$. Fig. 16 shows an example of the profile of the fatigue crack propagated from a notch root under imposed compression cycles. Crack growth occurs primarily along the carbide–binder interface. Note that there is no cracking whatsoever within the brittle carbide phase. These results imply that the mechanisms of cyclic fracture identified in ceramics also have significance to the failure of ceramic–metal composites under far-field cyclic compression.

## 5. Applications of fatigue crack growth in cyclic compression

The possibility of obtaining controlled and stable crack propagation in brittle solids even at room temperature makes the phenomenon of crack growth under cyclic compression a unique experimental technique for pre-cracking fracture toughness specimens. Currently practised testing procedures generally suffer from the shortcoming that the artefacts of the testing technique can strongly influence the measured or inferred values of fracture toughness as there is no unique way of developing a controlled, non-catastrophic "sharp" flaw (pre-crack) prior to fracture. For example, the widely practised indentation

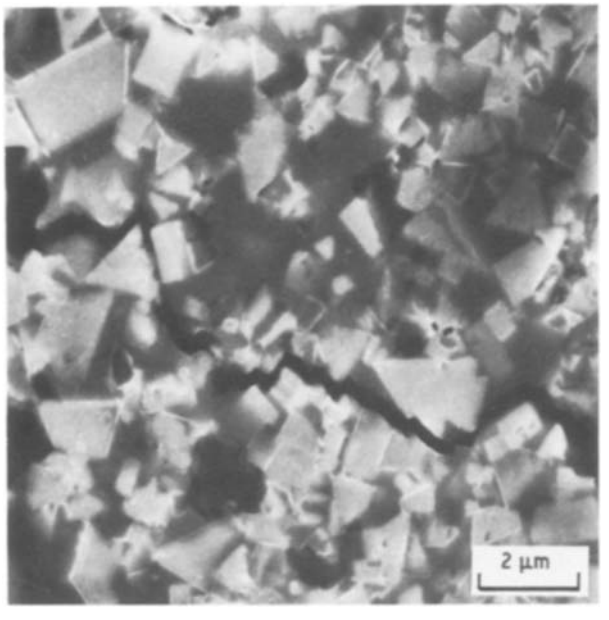


*Figure 16* Crack growth along the interface between the brittle carbide and metallic binder in WC–25 wt % Co cermet fractured under far-field cyclic compression.

techniques for fracture toughness measurements can produce multiple cracks as well as a residual zone of damage. Chevron notched (short-rod) specimens are not suitable for determining stable crack growth in materials exhibiting a resistance curve behaviour. The compression method outlined in this work provides an ideal pre-cracking procedure for fracture toughness tests for the following reasons:

1. Controlled and non-catastrophic crack growth can be obtained in brittle materials even at room temperatures. To our knowledge, this appears to be the only procedure capable of producing stable fatigue crack growth in brittle solids at low temperatures.
2. The total distance of crack growth under far-field cyclic compression can be suitably manipulated by controlling the load amplitude and load ratio. (Caution should be exercised in the determination of the choice of loads in brittle solids because an extremely small load amplitude in cyclic compression would not lead to any cracking, whereas an extremely large load amplitude can result in catastrophic failure during the very first cycle.)
3. As the crack decelerates and arrests naturally, the maximum extent of damage left at the tip of the crack grown (until arrest) under far-field cyclic compression is not likely to affect subsequent fracture toughness measurements. This assumption has been experimentally substantiated in metals.
4. The procedure for pre-cracking in cyclic compression can also be used in ceramic–ceramic composites [36] (e.g. SiC whiskers in an $Si_3N_4$ matrix) and in ceramic–metal composites [12, 19] (e.g. SiC whiskers in an aluminium matrix or a cemented carbide).
5. Our attempts (described below) to apply this technique for fracture toughness measurements in polycrystalline aluminium oxide confirm the viability of this technique.

In an attempt to study the use of the compression method for the measurement of fracture toughness in ceramics, a parallel study was conducted [37] where notched specimens of polycrystalline aluminium oxide (AD 995) were pre-cracked in cyclic compression. The specimen dimensions were: length = 50 mm, width $W$ = 10.5 mm, thickness = 5.2 mm. The notch geometry was similar to that in the experiments described in Figs 1 to 4. The plane of the notch was perpendicular to the length of the specimen. Subsequent to pre-cracking in compression, the side surfaces of the specimen were ground (about 0.5 mm on either side) to remove any crack front curvature near the free surfaces (see Fig. 4, for example). (An examination of the fracture surfaces after the test did reveal a straight crack front through the thickness of the specimen.) Following this, a quasi-static fracture test was conducted where the specimen was loaded in four-point bending (with the loading direction being parallel to the plane of the notch and perpendicular to the length of the specimen). Several experiments conducted in the polycrystalline materials produced consistent values of fracture toughness. The average fracture toughness values measured for AD 995 were 4.25 MPa $m^{1/2}$, and the maximum range of scatter was $\pm 0.25$ MPa $m^{1/2}$. These results demonstrate the viability of the compression method for producing well-controlled sharp flaws in brittle solids prior to fracture experiments. The distance between the inner loading points was $2W$ and the distance between the outer loading points was $4W$. The crack length to width ratio ($a/w$) was 0.512.

The ability to produce controlled, non-catastrophic sharp fatigue flaws under far-field cyclic compression also offers a unique experimental tool for obtaining fatigue/creep/stress corrosion thresholds and the entire range of crack growth rates from the threshold to the point of catastrophic fracture in a single specimen. This can be achieved by using the following procedure: (i) fatigue cracks are propagated from the notch-root under imposed cyclic compressive stresses, until complete crack arrest occurs; (ii) subsequently, the specimens are loaded in static tension or bending (for stress corrosion/creep studies) or cyclic tension or bending (for fatigue-creep studies) at a stress intensity or load marginally below the expected values of the threshold, (iii) the load is incremented until crack growth is detected and the entire crack-growth curve can be obtained by measuring the progressive increase in crack length at a constant load (or load amplitude). A recent study in metals by Christman and Suresh [38] has demonstrated that the maximum amount of damage left at the tip of a crack grown (and arrested) in plane strain cyclic compression is not large enough to affect subsequent crack growth in tension, thereby validating the use of the compression method for the applications proposed here. Although the potential success of this technique in brittle materials can only be substantiated after detailed experimental investigations, it seems to offer some distinct advantages over currently used methods.

## 6. Concluding remarks

We have demonstrated in this work the occurrence of stable fatigue crack growth at room temperature in notched plates of polycrystalline ceramics subject to fully compressive far-field cyclic loads. Various microscopic and continuum characteristics of fatigue are discussed and prominent mechanisms of failure are identified. Large imposed compressive stresses induce extensive inelastic deformation in the vicinity of the notch root. A zone of residual tensile stresses is created at the notch-tip if the deformation within the notch-tip process zone leaves permanent strains upon unloading from the maximum nominal compressive stress. This mechanism appears to be the principal driving force for Mode I crack growth in ceramics stressed in cyclic compression. The relative frictional sliding of the faces of the microcracks oriented at a certain angle to the compression axis may also produce, at their tips, intergranular tension cracks at an adjacent boundary oriented for the highest opening stress value. While the early compression cycles may cause appreciable damage in the form of microcracking at the root of the notch, the coalesence of microcracks to form a macroscopic Mode I fatigue flaw is achieved over tens of thousands of subsequent cycles. Intergranular fracture promotes the accumulation of debris within the cracks, a consequence of which is the

progressive development of closure in the wake of the advancing crack-tip leading to crack arrest. It is shown that crack growth from notches under far-field cyclic compression is a phenomenon exhibiting a macroscopically similar behaviour in a wide range of materials spanning the very ductile metals to extremely brittle solids; the micromechanisms underlying this effect, however, are very different among the various classes of materials. As the process zone in the vicinity of the crack-tip is completely surrounded by material elastically strained in compression, fatigue crack growth under far-field cyclic compression is an intrinsically stable phenomenon in both ductile and brittle solids. Several important applications of the phenomenon of controlled and self-arresting crack advance under far-field cyclic compression are recommended for the fracture (and tensile) fatigue testing of brittle solids. While this investigation has identified and modelled several key features pertinent to the micromechanics of fatigue fracture, further theoretical and experimental studies are needed to elucidate the mechanisms under far-field cyclic compression in terms of the effects of grain size, amorphous grain-boundary films, temperature, load range, mean stress and residual stresses arising from thermal contraction anisotropy in non-cubic ceramics.

## Appendix

As indicated earlier, residual tensile stresses at the notch-tip are expected to be generated upon unloading from a maximum far-field compressive stress in solids exhibiting a non-linear stress–strain curve and permanent strains after the removal of far-field stress (e.g., Fig. 13). The magnitude of such residual tensile stresses in notched plates of plastically-deforming solids subject to far-field cyclic compression was estimated by Suresh and co-workers [16, 17]. More recently, Brockenbrough and Suresh [33] developed a constitutive formulation to estimate the notch-tip residual stress patterns in microcracking brittle solids loaded in cyclic compression. The microcrack nucleation criterion was assumed to be

$$\beta = A\left(\frac{\bar{\sigma}}{\sigma_0} - 1\right)^n \quad \text{for } |\bar{\sigma}| > |\sigma_0|,\ \beta < \beta_s$$

$$\beta = 0 \quad \text{for } |\bar{\sigma}| \leqslant |\sigma_0|$$

else

$$\beta = \beta_s \tag{A1}$$

Here $\sigma_0$ is a threshold stress for microcracking, the microcrack density $\beta = Na^3$ where $N$ is the number of microcracks per unit volume and $a$ the radius of the penny shape crack, $\bar{\sigma}$ is an effective stress (defined by $\bar{\sigma}^2 = \underline{Q}\underline{Q}$), $A$ is a constant and $n$ is an exponent. Considering an isotropic elastic model and using the self-consistent estimates of Budiansky and O'Connell [39] for the loss in stiffness caused by randomly oriented, penny-shaped cracks, Brockenbrough and Suresh [33] conducted a numerical analysis of the notch-tip tensile stresses for microcracking ceramics fatigued in compression. The unloading behaviour was characterized in [33] by a parameter $\lambda$ (denoting the fraction of closed microcracks) such that $\lambda = 0$ when all the microcracks gradually close upon unloading from the maximum far-field compression stress (line B, Fig. 13); $\lambda = 1$ when all the microcracks are blocked from closing upon unloading (line C, Fig. 13) and $0 < \lambda < 1$ when only a fraction of the microcracks nucleated during the compression loading cycle close upon unloading (line D, Fig. 13).

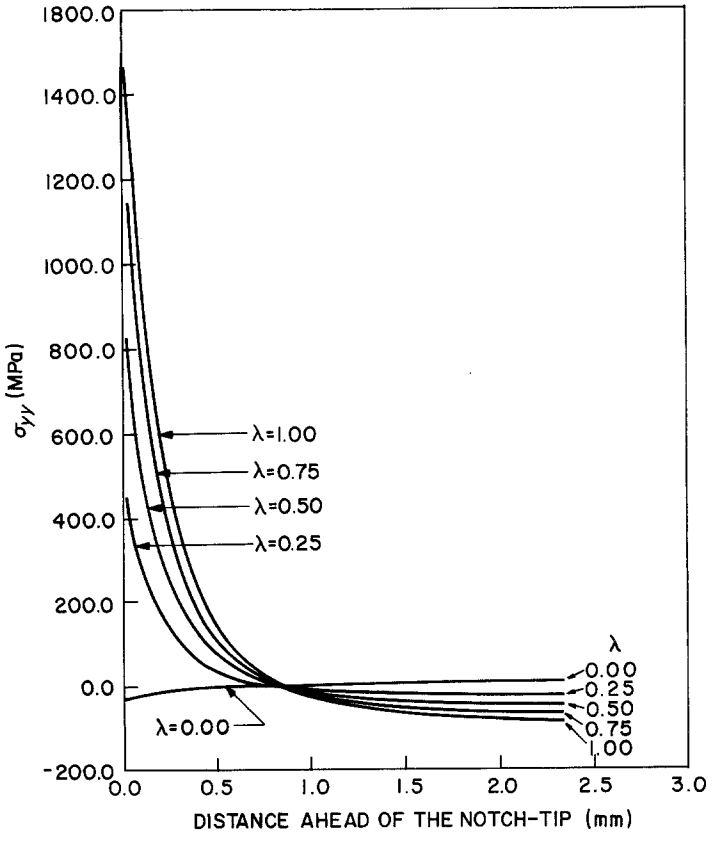


*Figure A1* Variation of the numerically-estimated near-tip normal stress $\sigma_{yy}$ on the plane of the notch as a function of the distance ahead of the notch-tip for the AD 995 notched plates unloaded from a maximum far-field compressive stress of −300 MPa.

For the single edge-notched specimen geometry of the AD 995 polycrystalline $Al_2O_3$ used in this work, the notch-tip residual stresses after unloading from the first compression cycle were estimated by Brockenbrough and Suresh [33] for a stress range of 0 to $-300$ MPa, $|\sigma_0| = 30$ MPa, $A = 0.004$, $n = 1$ and $\beta_s = 0.4$. Fig. A1 shows the variation of numerically estimated normal stress $\sigma_{yy}$ on the plane of the notch as a function of the distance from the notch-tip (for various values of $\lambda$) after fully unloading from the maximum compressive stress. It is evident that when $\lambda > 0$, residual tensile stresses are generated at the notch-tip. For the limiting case of $\lambda = 1$, the notch-tip is subjected to a *tensile* stress of about 1400 MPa upon unloading from a maximum compressive stress of $-300$ MPa. Considering that the tensile fracture strength (reported by the supplier) of AD 995 is of the order of 260 MPa, it is obvious that the residual tensile stresses are of sufficient magnitude to promote Mode I fracture ahead of the notch-tip. In this context, we note that the distance ahead of the notch-tip ($\sim 0.3$ mm) over which the near-tip tensile stress exceeds the tensile fracture strength of AD 995 is comparable to the total distance of crack growth observed under far-field cyclic compression. The magnitude of the tensile stresses predicted by the numerical model in [33] is sensitive to the parameters in (A1) as well as the constitutive model for $\bar{\sigma}$. However, the analysis does provide a clear mechanistic justification for the growth of Mode I fatigue cracks under fully compressive far-field cyclic loads. It is this local zone of residual tension at the notch-tip which appears to be the "driving force" for stable fatigue crack growth at room temperature in a direction macroscopically normal to the compression axis.

The residual tensile stresses shown in Fig. A1 are relevant to the particular case of a microcracking brittle solid; we emphasize, however, that similar trends would be observed for a material exhibiting non-linear deformation behaviour (as in Fig. 13) in response to plasticity or phase transformation. For example, it is known that transformation-toughened ceramics (partially-stabilized $ZrO_2$) exhibit extensive inelastic deformation in compression where permanent strains are retained upon removal of the compressive load (e.g., [40, 41]). Recently, Suresh and Sylva [42] have experimentally shown that the application of cyclic compressive stresses to notched specimens of partially-stabilized $ZrO_2$ can lead to appreciable Mode I cracking. Fig. A2 shows an example of a Mode I fatigue crack emanating from the notch-tip in a $ZrO_2$–4.5 wt % $Y_2O_3$ ceramic (supplied by Zircar, Inc., Florida, New York). The general characteristics of the compression fatigue effect in this material are similar to those described earlier for polycrystalline $Al_2O_3$.

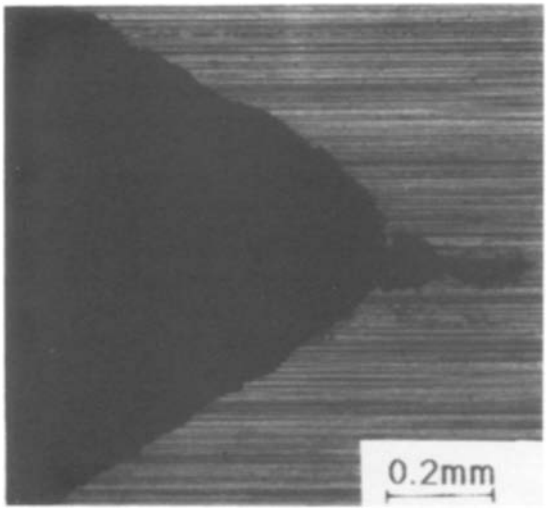


*Figure A2* An example of a Mode I fatigue crack growth in a $ZrO_2$–4.5 wt % $Y_2O_3$ ceramic loaded in cyclic compression. The compression axis is vertical (after Suresh and Sylva [42]).

## Acknowledgements

This work was supported partly by the National Science Foundation under Grant NSF-ENG-8451092 and partly by a grant from the Aluminium Company of America to Brown University. The use of the Central Mechanical Testing Facilities of the Materials Research Laboratory at Brown University is gratefully acknowledged. We express our sincere thanks to Mr Chris Bull for his help in setting up some of the experiments. It is a pleasure to acknowledge Mr John Brockenbrough for his comments and Mrs Louise Gray for her help in preparing this manuscript. S. S. acknowledges the US Department of Energy Contract DE-FG 0284ER45167 which supported the initial work on the topic of compression fatigue.

## References

1. A. G. EVANS, A. H. HEUER and D. L. PORTER, in "Fracture 1977", edited by D. M. R. Taplin (University of Waterloo Press, Waterloo, 1977) p. 529.
2. D. A. KROHN and D. P. H. HASSELMAN, *J. Amer. Ceram. Soc.* **55**, (1972) 208.
3. F. GUIU, *J. Mater. Sci. Lett.* **13** (1978) 1357.
4. CHEN and KNAPP, in "Fracture Mechanics of Ceramics 2", edited by R. C. Bradt, D. P. H. Hasse and F. F. Lange (Plenum Press, New York, 1974) p. 691.
5. S. ITO, Y. YAMAUCHI, M. ITO and S. SAKAI, in "Proceedings of Japan Conferences on Materials Research", Vol. 26 (Tokyo, 1983) p. 270.
6. A. G. EVANS and M. LINZER, *Int. J. Fract.* **12** (1976) 217.
7. A. G. EVANS and E. R. FULLER, *Metall. Trans.* **5A** (1974) 27.
8. A. G. EVANS, L. R. RUSSELL and D. W. RICHERSON, *ibid.* **6A** (1975) 707.
9. J. RITTER, in "Fracture Mechanics of Ceramics", edited by R. C. Bradt, A. G. Evans, D. P. H. Hasselman and F. F. Lange, Vol. 4 (Plenum Press, New York, 1983) p. 667.
10. A. G. EVANS, *Int. J. Fract.* **16** (1980) 485.
11. L. EWART and S. SURESH, *J. Mater. Sci. Lett.* **5** (1986) 774.
12. S. SURESH and L. A. SYLVA, *Mater. Sci. Eng.* **83** (1986) L7.
13. "Fracture in Compression of Brittle Solids", edited by A. S. Argon, National Materials Advisory Board Report NMAB-404 (National Academy Press, Washington, DC, 1982).
14. R. P. HUBBARD, *J. Basic Eng.* **91** (1969) 625.
15. S. SURESH, *Eng. Fract. Mech.* **21** (1985) 453.
16. S. SURESH, T. CHRISTMAN and C. BULL, in "Small Fatigue Cracks," edited by R. O. Ritchie and J. Lankford (Metallurgical Society of AIME, Warrendale, Pennsylvania, 1986) p. 513.
17. D K. HOLM, A. F. BLOM and S. SURESH, *Eng. Fract. Mech.* **23** (1986) 1097.
18. J. R. RICE, ASTM STP 486, (American Society for Testing and Materials, Philadelphia, 1967) p. 247.

19. P. ASWATH and S. SURESH, research in progress (1986).
20. A. H. HEUER, *Phil. Mag.* **13** (1966) 379.
21. R. W. RICE, *Mater. Sci. Res.* **5** (1971) 195.
22. J. LANKFORD, *J. Mater. Sci.* **12** (1977) 791.
23. S. M. WIEDERHORN, B. J. HOCKEY and D. E. ROBERTS, *Phil. Mag.* **28** (1973) 783.
24. A. G. EVANS, S. M. WIEDERHORN and B. J. HOCKEY, *J. Mater. Sci.* **9** (1974) 1367.
25. D. W. JOHNSON and P. GIBBS, *J. Appl. Phys.* **34** (1963) 2852.
26. A. G. EVANS, *Acta Metall.* **26** (1978) 1845.
27. R. W. RICE, S. W. FREIMAN and P. F. BECHER, *J. Amer. Ceram. Soc.* **64** (1981) 345.
28. P. L. PRATT, *Metal Sci.* **14** (1980) 363.
29. W. R. BUESSEM and F. F. LANGE, *Interceram* **15** (1966) 229.
30. J. E. BLENDELL and R. L. COBLE, *J. Amer. Ceram. Soc.* **65** (1982) 174.
31. Y. FU, PhD. thesis, University of California (1983).
32. H. TADA, P. C. PARIS and G. R. IRWIN, "The Stress Analysis of Cracks Handbook" (Del Research Corporation, Hellertown, Pennsylvania, 1973).
33. J. BROCKENBROUGH and S. SURESH, Brown University Report No. MSM-8451092/1 (September 1986).
34. F. A. MCCLINTOCK and J. B. WALSH, in Proceedings of 4th US National Congress on Applied Mechanics (American Society of Mechanical Engineers, New York, 1962) p. 1015.
35. S. NEMAT-NASSER and H. HORII, *J. Geophys. Res.* **87** (1982) 6805.
36. S. SURESH and X. HAN, unpublished results (1986).
37. S. SURESH, L. EWART, M. MADEN, W. SLAUGHTER and M. NGUYEN, *J. Mater. Sci.* **22**(3) (1987).
38. T. CHRISTMAN and S. SURESH, *Eng. Fract. Mech.* **23** (1986) 953.
39. B. BUDIANSKY and J. O'CONNELL, *Intl. J. Solid Struct.* **12** (1976) 81.
40. J. LANKFORD, *J. Amer. Ceram. Soc.* **66** (1983) C-212.
41. I. W. CHEN, *ibid.* **69** (1986) 181.
42. S. SURESH and L. A. SYLVA, Brown University Report No. MSM-8451092/2 (October 1986).

*Received 28 April*
*and accepted 21 July 1986*